TITLE

Convergent impact of schizophrenia risk genes

AUTHORS

Kayla G. Townsley*[1,2,3] Aiqun Li*[1,2], PJ Michael Deans[1,2,4], John F. Fullard[1,3,4,5], Alex Yu[1,2], Sam Cartwright[1,2], Wen Zhang[1,2,3], Minghui Wang[1,2], Georgios Voloudakis[1,3,5], Kiran Girdhar[1,2,3,5], Eli Stahl[1,3], Schahram Akbarian[2,3], Bin Zhang[1,2], Panos Roussos[1,2,3,5,6,7], Laura M. Huckins[1,3,4,8#], Kristen J. Brennand[1,2,3,4,9.10#]

AFFILIATIONS

[1] Pamela Sklar Division of Psychiatric Genomics, Department of Genetics and Genomics, Icahn Institute of Genomics and Multiscale Biology, Icahn School of Medicine at Mount Sinai, New York, NY 10029

[2] Nash Family Department of Neuroscience, Friedman Brain Institute, Icahn School of Medicine at Mount Sinai, New York, NY 10029

[3] Department of Psychiatry, Icahn School of Medicine at Mount Sinai, New York, NY 10029

[4] Department of Psychiatry, Division of Molecular Psychiatry, Yale University School of Medicine, New Haven, CT 06511

[5] Center for Disease Neurogenomics, Icahn School of Medicine at Mount Sinai, New York, NY 10029, USA

[6] Illness Research Education and Clinical Center (VISN 2 South), James J. Peters VA Medical Center, Bronx, 10468, NY, USA

[7] Center for Dementia Research, Nathan Kline Institute for Psychiatric Research, Orangeburg, NY 10962, USA

[8] Seaver Autism Centre for Research and Treatment, Icahn School of Medicine at Mount Sinai, New York, NY 10029, USA

[9] Department of Genetics, Yale University School of Medicine, New Haven, CT 06511

[10] Wu Tsai Institute, Yale University School of Medicine, New Haven, CT 06511

* These authors contributed equally to this work.

Correspondence:

kristen.brennand@yale.edu and laura.huckins@yale.edu

Number of Tables: 2
Number of Boxes: 1
Number of Figures: 5

ABSTRACT

Genetic liability associated with schizophrenia most frequently arises from common genetic variation that confers small individual effects and contributes to phenotypes only when considered in aggregate. These risk variants are typically non-coding and act by genetically regulating the expression of one or more gene targets (eGenes), but the mechanisms by which unlinked eGenes interact to contribute to complex genetic risk remains unclear. Here we apply a pooled CRISPR approach to evaluate in parallel ten schizophrenia eGenes in human glutamatergic neurons. Querying the shared neuronal impacts across eGenes reveals shared downstream transcriptomic impacts (“convergence”) concentrated on pathways of brain development and synaptic signaling. The composition and strength of convergent networks is influenced by both the similarity of eGene functional annotation and the strength of eGene co-expression in human postmortem brain tissue. Convergent networks resolve distinct patterns of eGene up-regulation associated with individual-level risk in the post-mortem dorsolateral prefrontal cortex that are broadly enriched for neuropsychiatric disorder risk genes and may represent molecular subtypes of schizophrenia. Convergent gene targets are druggable as novel points of therapeutic intervention. Overall, convergence suggests a model to explain how non-additive interactions arise between risk genes and may explain cross-disorder pleiotropy of genetic risk for psychiatric disorders.

KEYWORDS

schizophrenia; psychiatric genomics; human induced pluripotent stem cells; CRISPR-screen; neurons

INTRODUCTION

Genome-wide association studies (GWAS) of single nucleotide polymorphisms (SNPs) continue to identify loci (250 and growing[1-3]) that are significantly associated with risk for schizophrenia (SCZ). These common variant risk loci regulate expression of target genes (eGenes) in pyramidal excitatory neurons (and a subset of GABAergic interneurons)[4,5], particularly synaptic pathways[6,7]. Risk genes are expressed during fetal cortical development[8,9], highly co-expressed in human brain tissue[10] and cultured neurons[11], and show high connectivity in protein-protein interaction (PPI) networks[11-13]. Transcriptomic studies of SCZ post-mortem brains likewise identify common downregulation of neuronal and synaptic genes as well as upregulation of immune genes in astrocytes[14,15]. An unanswered question is whether individual risk variants sum linearly[16,17] or whether they are amplified[18] or buffered[19] by epistatic interactions. Here we ask how the neuronal impact(s) of risk genes converge in a common genetic background. Identifying the regulatory node(s) downstream of risk genes could reveal novel SCZ biology and point to new therapeutic targets.

CRISPR-mediated genetic perturbation of SCZ eGenes in human induced pluripotent stem cell (hiPSC)-derived neurons can definitively reveal their causal impact on gene expression, cellular function, and synaptic activity[20-23]. Such genetic studies were typically conducted in a one-gene-at-a-time manner requiring a substantial time and resource investment, but state-of-the-art CRISPR screens now incorporate a pooled multiplexed design, minimizing experimental variability, increasing the power of the associated analyses, and more closely recapitulating the observed polygenic architecture of disease risk. Recent studies queried an overlapping set of highly penetrant loss-of-function ASD genes *in vitro* in human neural progenitor cells (27 genes)[24] and human brain organoids (3 and 36 genes)[25,26], and *in vivo* in fetal mouse brains (35 genes)[27] and *Xenopus tropicalis* (10 genes)[28], reporting convergence impacting neurogenesis[24,25,27,28], WNT signaling[24], and gene expression[25,27]. This approach has not yet been applied to SCZ genes, loss-of-function[29] or otherwise. More critically, the convergent impact of common risk variant target genes – perturbations of which are frequently inherited together, and the impacts of which are apparent only in aggregate –are unknown.

We previously integrated hiPSC-based models with CRISPR activation (CRISPRa) and interference (CRISPRi) technologies to study four top-ranked putative GWAS eGenes associated with SCZ (*FURIN, SNAP91, TSNARE1, CLCN3*). Our observations revealed that combinatorial perturbation of these risk genes resulted in downstream effects that could not be predicted from individual perturbations alone and that were enriched for synaptic as well as common and rare SCZ genes[30]. These synergistic effects emphasize the importance of considering the polygenic nature of SCZ, where a combination of variants contributes to risk.

While CRISPR screens have improved our ability to perturb multiple genes in parallel, they currently lack the capacity to consider all known or predicted SCZ eGenes in a single experiment. Thus, it is crucial to identify methods to explore

convergence across experiments – here we work with a subset of schizophrenia eGenes across two CRISPRa screens at two developmental timepoints to explore the utility of Bayesian bi-clustering to identify biologically meaningful convergence across gene sets and experiments. We resolved the convergent impact of ten eGenes with strong evidence of genetic regulation by Psychiatric Genomics Consortium (PGC3)-SCZ GWAS loci and orthogonal epigenetic data supporting their up-regulation: *CALN1, CLCN3, FES, NAGA, PLCL1, SF3B1, TMEM219, UBE2Q2L, ZNF823, ZNF804A*. Two independent pooled single-cell RNA-sequencing CRISPRa-based experiments[31] revealed the genome-wide transcriptomic consequences of activating SCZ eGene expression at two developmental timepoints (day 7 or day 21) in human *NGN2*-induced glutamatergic neurons (**Fig. 1**)[32,33]. These ten SCZ eGenes demonstrated shared and distinct downstream effects, independent of their previously annotated biological roles (**Supplemental Data 1**). Convergent genes downstream of all ten targets were enriched for known common and rare risk genes broadly associated with psychiatric disorders, transcription factors previously implicated in the regulation of these target genes, and biological pathways involved in SCZ etiology, such as synaptic signaling (**Fig. 2**). The ability and degree of convergence within a network was, in part, influenced by the degree of functional similarity between perturbed target genes and the correlation strength of their expression in post-mortem dorsolateral prefrontal cortex (DLPFC) (**Fig. 3**). Network reconstruction for convergent signatures matched to eGene up-regulation patterns in the post-mortem dorsolateral prefrontal cortex (DLPFC) resolved distinct networks of SCZ risk at the individual level, which may represent molecular sub-types of SCZ (**Fig. 4**). Overall, Bayesian bi-clustering resolved convergent signatures across two independent lists of SCZ eGenes manipulated in two distinct ECCITE-seq[31] experiments. The cross-disorder enrichment of convergent targets for psychiatric risk genes suggests they underlie shared clinical hallmarks and pleiotropy of risk.

RESULTS

Prediction and prioritization of brain genes activated by SCZ GWAS loci.

Common SCZ-associated risk loci are highly enriched in *cis*-regulatory elements, including promoters and enhancers, and frequently regulate the expression of one or more eGenes[34-36] as cis- or *trans*-acting expression quantitative trait loci (eQTLs)[37]. Transcriptomic imputation studies predict trait-associated genetically regulated gene expression by combining large-scale genetic data (GWAS summary statistics) with tissue-specific eQTL reference panels[38-40]. These approaches infer physiological consequences of GWAS association statistics, conferring magnitude, directionality, and tissue-level precision. eGenes (i.e., genes with an associated eQTL) whose brain expression was predicted to be up-regulated by PGC3-SCZ GWAS SNPs[3] were selected by two complementary approaches. Each list of genes was used to design, construct, and validate a distinct gRNA library.

First, transcriptomic imputation was considered together with the strength of co-localization between GWAS risk loci and brain eQTL peaks to identify: *CALN1*,

CLCN3, CUL9, DOC2A, PLCL1, INO8E0, SF3B1, SNAP91, TMEM219, and ZNF823. Post-mortem CommonMind Consortium (CMC)[41] and PGC3-SCZ GWAS[3] data was leveraged to calculate predicted differential expression in brain (using PrediXcan[40]; 623 CMC samples), and colocalization of fine-mapped GWAS and eQTL associations (using COLOC[37,42]; 537 EUR-CMC samples; 65,205 cases and 87,919 controls GWAS). Our analysis yielded ~250 genes with significant ($p<6x10^{-6}$)[40] predicted differential expression between SCZ-cases and controls using PrediXcan and 25 loci with very strong evidence (PP4>0.8) of colocalization of PGC3-GWAS loci and brain eQTLs; there was significant overlap between the two analyses (22/25 COLOC genes were PrediXcan significant; binomial test p-value $3.03x10^{-112}$). Overall, SCZ eGenes were prioritized from PGC3-GWAS[3] based on: i) significant genetic up-regulation (**Table 1**), ii) colocalization of GWAS and eQTL associations, iii) exclusion of genes located in the MHC locus, iv) robust expression in our hiPSC neuron RNAseq (**Table 1**). Although ten top coding genes were selected, only four were subsequently robustly detected by scRNAseq (see below).

Second, transcriptome and epigenome imputation were performed for SCZ to prioritize: *NEK4, PLCL1, UBE2Q2L, NAGA, FES, CALN1,* and *ZNF804*. The PsychENCODE transcriptome datasets of genotyped individuals (brain homogenate, n=924)[14,43] were leveraged to impute brain transcriptomes at the level of genes and isoforms with EpiXcan[44]; EpiXcan increases power to identify trait-associated genes under a causality model by integrating epigenetic annotation[45]. In addition, we used PrediXcan[40] to perform epigenomic activity imputation for H3K27ac (brain homogenate, n=122; neuronal, n=191) and H3K4me3 (neuronal, n=163)[46] to more confidently identify *cis* regulatory elements associated with risk for SCZ. Overall, SCZ eGenes were prioritized from PGC3-GWAS[3] based on: i) significant genetic up-regulation of expression (z-score >6 for genes; (**Table 2**), ii) epigenetic support (>1 epigenome assay with association within the promoter of the gene) (**Table 2**), iii) exclusion of genes located in the major histocompatibility complex (MHC) locus, thus, prioritizing genes that had orthogonal data supporting up-regulation. Six top coding genes and one top pseudo-gene were selected; six of the seven targets were subsequently robustly detected by scRNAseq (see below).

A pooled CRISPRa approach to resolve the transcriptomic effects of SCZ eGenes at two developmental time-points in human excitatory neurons.

Fusion of a catalytically inactive dCas9 to the tripartite activator VP64-p65-Rta (VPR)[47,48] achieves efficient up-regulation in hiPSC neurons[49]. Coupling CRISPR screening to single-cell RNA sequencing readouts yields rich, high-dimensional phenotypes from pooled screens and permits direct detection of sgRNAs (Expanded CRISPR-compatible CITE-seq, ECCITE-seq)[31].

To evaluate the impact of the twelve SCZ prioritized genes, two independently designed, constructed, and validated pooled CRISPRa libraries were transduced into *NGN2*-neurons from two donors in independent experiments (three XY donors of European ancestry with no history of psychiatric diagnoses and median-level polygenic risk scores for SCZ) at unique developmental time-points.

First, three sgRNAs were designed for each of the ten SCZ eQTL genes (*CALN1*, *CLCN3, CUL9, DOC2A, PLCL1, INO8E0, SF3B1, SNAP91, TMEM219, ZNF823).* gRNAs were individually cloned for expression from our LV expression vector[49], expressed in arrayed format, and validated by qPCR. In the case of genes with multiple promoters, gRNAs were designed to target the promoter for the primary transcript listed on the NCBI entry. The gRNAs with validated expression predicted to mimic the strength of the eQTL effect most closely was selected. Individual gRNAs were packaged as lentiviruses and titered prior to pooling**.** An sgRNA library targeting promoters (low MOI, ~300 cells/sgRNA) was used to generate strong-effect up-regulation and maximize detection of trans effects. Second, a pooled library of ten sgRNAs for each of the seven SCZ EpiXcan eGenes was designed (*NEK4, PLCL1, UBE2Q2L, NAGA, FES, CALN1, ZNF804A*: 10 gRNAs each), and combined with 1 scramble gRNA negative control previously functionally validated by CRISPRa[30]. The synthesized, annealed, and pooled gRNAs were cloned into a lentiviral expression vector (lentiGuide-Hygro-mTagBFP2)[49]. To validate the pooled sgRNA library, an innovative and more accurate method to determine individual sgRNA abundance was developed. Note that the 20-bp gRNA sequences are the only different small parts in the ~8,000 bp expression plasmid. DNA fragmentation by sonication yields redundant and repetitive DNA fragments that are not of interest. To increase the probability of getting sequences of the specific gRNAs, the gRNA library was digested with two restriction enzymes to yield a ~378 bp DNA fragment containing different gRNAs. Following Illumina's protocol for library preparation, index adapter sequences were added to the ends of a DNA fragment for MiSeq (25 million sequencing reads and 2× 250 bp read lengths). After confirming the equal distribution of individual gRNA within the library, it was packaged into lentivirus and titrated.

After maturation, 7-day-old (7-gene) and 21-day-old (10-gene) *NGN2*-neurons were dissociated to single cell suspensions with papain, and bar-coded single cell cDNA generated using 10X Genomics Chromium. Normalization and downstream analysis of scRNA-seq data were performed using the Seurat R package (v.2.3.0), which enables the integrated processing of multimodal single-cell datasets. A Wilcox rank-sum test for upregulated gene expression was performed on demultiplexed cells for each experiment individually, with of the 12 resolvable target genes compared to their matched scramble control targeted cells. Of the 12 genes, 6 genes showed significant up-regulation and 4 genes showed nominally significant upregulation (**Supplemental Fig. 6C-D, Supplemental Table 2**).

Overall, we resolved cell perturbations of four of the ten SCZ eQTL eGenes (three unique gRNAs each) and six out of SCZ EpiXcan eGenes (ten unique gRNAs each). The inability to resolve all ten of the perturbations in the day 21 *NGN2*-neurons may reflect the difference in gRNA number used to target the eGenes, suggesting that either more cells and/or more gRNAs per target is necessary to resolve all ten perturbations. Overall, scRNA-seq on 8055 and 6697 cells respectively were adequate to resolve: the sgRNA in each cell, the *cis* target gene with differential expression, and the downstream *trans* alterations to

pathways resulting from initial *cis* up-regulation. Following QC and normalization, ten successful perturbations across both experiments were identified, with an average of 316 cells per perturbation or scramble control (ranging from 93-552) for a total of 3640 perturbed cells and 210 scramble controls (**Supplemental Fig. 3-6**). Upregulation of eGenes by CRISPRa ranged from 0.2 to 3. Log Fold-Change (LogFC), comparable to the dosage effects of the top predicted causal SNPs in the post-mortem DLPFC (LogFC range 0.3-5.2) (**Supplemental Table 2, Supplemental Fig. 6**).

Downstream transcriptomic impacts across ten SCZ eGenes perturbations converge on common and rare variant targets.

Successful CRISPR-activation of ten SCZ eGenes were significantly upregulated compared to controls (impacted the global transcriptome of 7-day-old (DIV7) and/or 21-day-old (DIV21) *NGN2*-excitatory neurons respectively and revealed shared and distinct effects (**Supplemental Fig. 7, Supplemental Table 1**). While *NGN2*-induction yields diverse excitatory neuron subtypes[50], there was no significant difference in the degree of variance between experiments (DIV7 or DIV21) and imputed cell fractions were not correlated with perturbation status (**Supplemental Fig. 1 and 2**).

Target-Convergent gene co-expression Networks (TCN) were built using an unsupervised Bayesian biclustering model (3850 cells, 16851 genes, batch corrected and normalized). Across all ten eGene perturbations, 1048 protein-coding source node genes (>5 edges) where identified, with a total network membership of 2418 genes that clustered together in at least 20% of the runs (**Supplemental Table 3**). Functional annotation of these network node genes identified significant enrichments for gene targets of SCZ GWAS common variants and transcription factors know to regulate SCZ risk genes, such as *AP4* (TFAP4)[51], *NFAT*[52], *ERR1*[53], and *TCF4*[54,55] (**Fig. 2C).** The cross-target convergent network was enriched in biological pathways implicated in SCZ etiology, with the top 50 node genes significantly enriched for GABAergic synapse (G.O; padj=2.62e-3), TYROBP Causal Network (WikiPathways; padj=7.36e-4), and estrogen response (Hallmark; padj=6.89e-3) genes. Over Representation Analysis (ORA) revealed SCZ, bipolar disorder (BIP), intellectual disability (ID), and autism spectrum disorder (ASD) common and rare variants to be significantly over-represented in node genes shared across all ten eGene perturbations (**Fig. 2C; Supplemental Table 4**).

Separation of these ten SCZ eGenes based on either signaling (**Fig. 2A**) or regulatory (**Fig. 2B**) function resolved unique convergent networks with no overlap in node genes (**Fig. 2E**), suggesting that the functionally similarity of SCZ eGenes affects downstream convergence. Each of these networks included distinct genes annotated for synaptic and immune signaling function, as well as neuropsychiatric GWAS target genes (**Supplemental Table 4**).

Convergent downstream impacts are influenced by functional similarity of SCZ eGenes.

Downstream convergent effects of eGene perturbations increases with biological specificity based on shared function and network connectivity. We calculated the functionally similarity and degree of network convergence following network reconstruction across combinations of eGene CRISPRa-perturbations (1003 sets). Functionally similarity scores were calculated using Gene Ontology (GO) score (within Biological Pathway (BP), Cellular Component (CC), and Molecular Function (MF)[56], DLPFC score (strength of the correlation in gene expression in the postmortem brain), and Signaling Score (SS) (proportion of eGenes with annotated function as "signaling" (see **Methods**, **Box 1**, **Supplemental Fig. 8**). Here we define "convergence" as the independent development of transcriptomic similarities between separate gene perturbations that move towards shared biological function, "degree of convergence" as the sum of the network connectivity score and "average functional similarity of network genes" based on Gene Ontology semantic similarity scoring (**Box 1**).

Of the 1003 random sets tested, 64.8% resolved a convergent network passing at least a 10% duplication threshold across 40 runs (**Fig. 3E**). While some networks demonstrate shared convergence, unique set combinations resolved distinct networks (**Fig. 3A**). DLPFC and Signaling scores were nominally positively correlated with network convergence degree across all sets (**Supplemental Fig. 4F**). Principal components analysis (PCA) across set functional scores, sample size, and the corresponding network convergence scores revealed the influence of set functional similarity and DLPFC co-expression on network convergence (Fig. 3B-D; **Supplemental Fig. 9,10**). Overall, functional scores influence convergence, notably the proportion of signaling eGenes represented in a set and the gene expression correlation strength in the postmortem DLPFC.

Finally, we asked if any genes (or gene pairs) were necessary or sufficient to resolve convergent networks. Intersection of genes represented in functionally similar sets over an increasing number of genes found that gene pairs *FES* and *NAGA*, and *ZNF804A* and *ZNF823* were sufficient to resolve low level convergence, while *NAGA* appears necessary to resolve convergence across *CALN1*, *CLCN3*, *FES*, *SF3B1*, and TMEM219 (**Fig. 3F**). Overall, using set intersections to identify sufficiency and necessity indicates an important role for *NAGA* in the ability to resolve convergence across this set of SCZ eGenes.

CRISPR screens can model individual-level risk associated with psychiatric diagnoses and resolve novel convergent networks.

Clustering (K-means) of post-mortem DLPFC gene expression data (CMC, n=991) identified individuals with shared patterns of upregulation in these 10 SCZ eGenes; the average Z-scores of each target gene across all clusters is reported in **Supplemental Table 5**. Targets within each cluster with Z-score >= +0.5 were assigned as perturbed (**Fig. 4A**). Clusters based on target eGene expression were significantly different based on the diagnosis status of individuals within a cluster (Pearson's Chi-squared; X^2=140, df=21, p-value=9.51e-20) (e.g., cluster 8, SCZ, X^2=3.286; cluster 12, affective disorders (AFF), X^2=5.57), cluster 16, control, X^2=3.014) (**Fig. 4C**). Target-convergent network reconstruction was run

in our scRNA-seq data for sets of eGenes based on the DLPFC cluster perturbation assignments. (**Fig. 4B**).

We modeled the patterns of upregulation present in the post-mortem DLPFC, representing individual level risk, in *NGN2*-neurons and identified unique convergent networks (**Fig. 4D-E**) an approach that may help identify molecular subtypes within diagnostic groups in the future. For example, CMC clusters associated with SCZ (Cluster 8) compared to general affective disorders (AFF) (Cluster 12) revealed distinct convergent networks with unique node genes. Of note, the central protein-coding node gene of the cluster 12 network is *ABCG2*—down-regulated in a subset of SCZ cases with a neuroimmune molecular subtype (SCZ Type II)[57,58], a biomarker associated with increased negative symptoms[59], and associated with SCZ treatment resistance[60].

Prediction and empirical validation of drugs predicted to reverse convergent signatures in neurons.

We identified drugs predicted to manipulate top node genes[61]. Across all eGene perturbations, reversers of convergent node signatures were enriched for mechanisms previously associated with psychiatric disorders, including HDAC inhibitors[62] (normalized connectivity score (NCS)=-1.63; FDR adjusted pval<0.08), ATPase inhibitors[63] (NCS)=-1.61; FDR<0.08)], and sodium channel blockers[64] (NCS=-1.59; FDR<0.08). Mimickers of convergent node signatures were enriched for pathways associated with stress response, including glucocorticoid receptor agonists (NCS=1.66, FDR<0.08) and NFKB pathway inhibitors (NCS=1.60; FDR<0.2). (**Fig. 5B, Supplemental Table 6**). Nominally significant enrichments were only identified in non-neuronal cell lines and may point to cell-type specific responses to these drugs that do not reflect their effects on neuronal cells.

We prioritized three drugs that reversed signatures specifically in neurons (see **Methods**, **Fig. 5A**). Anandamide, a cannabinoid receptor agonist, was predicted as a reverser of the 10-eGene convergent network signature (NCS=-1.38, FDR=1) as well as the individual signature of *CALN1* (NCS=-1.23, FDR=0.16). This is notable as the endocannabinoid system has been independently hypothesized to be a therapeutic target[65] and shown to alleviate psychosis[66]. Simvastatin reverses the convergent network signature (NCS=-1.14, FDR=1) and *TMEM219* perturbation (NCS=-0.8823, FDR=0.26), and has been associated with a reduction of negative symptoms[67] and symptom severity[68] in SCZ. Etomoxir reverses the signatures of the 10-eGene convergent network (NCS=-1.35, FDR=1), *CALN1* (NCS=-1.42, FDR=0.04) and *TMEM219* (NS=-1.09, FDR=0.01). An inhibitor of fatty acid oxidation (FOA) through inhibition of carnitine palmitoyl transferase 1 (CPT1a), it is notable that elevated levels of acyl-carnitines are a biomarker for metabolic syndrome, which affects patients with SCZ at a higher rate than the general population[69].

These prioritized drugs were tested *in vitro* for their ability to reverse, or oppose, the effects of paired SCZ eGene perturbations. CRISPRa for eGenes *CALN1* and *TMEM219* was performed in *NGN2*-neurons treated with their matched

reverser drugs (anandamide and etomoxir; simvastatin and etomoxir, respectively). Downstream transcriptomic and phenotypic assays were assessed to resolve eGene-drug effects on neuronal molecular, morphological, and physiological phenotypes (**Supplemental Fig. 11**). Notably, etomoxir significantly reduced neurite length (Adj. Pval=0.0162), an effect that was significantly opposed by *CALN1* perturbation (Adj. Pval=0.008) (**Fig. 5C-E**) and was nominally opposed by *TMEM219* perturbation (Adj. Pval=0.082) . Thus, it is possible to pharmacologically target convergent effects, even when SCZ eGenes themselves are not druggable.

DISCUSSION

We report a CRISPR screen of putative SCZ GWAS target genes. Unlike recent studies of rare highly penetrant loss-of-function genes associated with ASD, our gene targets confer individually small effects that combine to yield clinically relevant impacts only in aggregate. A multiplexed CRISPR-based approach of ten SCZ eGenes (*CALN1, CLCN3, FES, NAGA, PLCL1, SF3B1, TMEM219, UBE2Q2L, ZNF823, ZNF804A*) in human glutamatergic neurons uncovered a convergent effect concentrated on neurodevelopmental pathways, synaptic transmission, and voltage-gated ion channel activity. Our results indicate that the functional similarity of target genes impacts the degree of convergence, suggesting that risk variants sum in different patterns and with greater specificity depending upon the extent to which their target genes converge within the same biological pathways[70]. However, the role of functional similarity in the epistatic interactions of common variant target genes needs to be investigated further. Applying these methods to a larger set of genes may yield greater insight into the role functional similarity plays in mediating the additive effects of polygenicity.

Overall, convergent signatures enriched for SCZ biology were observable across two independent lists of SCZ-GWAS target genes manipulated in two distinct ECCITE-seq experiments. Two independent pooled single-cell RNA-sequencing CRISPRa-based experiments[31] were applied to resolve the genome-wide transcriptomic consequences of activating SCZ eGene expression in two distinct sets of genes, at two developmental timepoints (day 7 or day 21) in human *NGN2*-induced glutamatergic neurons across three donors and generated either directly from hiPSCs or instead from hiPSC-derived neural progenitor cells (NPCs)[32,33]. Downstream convergent effects of target eGene perturbations matching patterns of up-regulation in the brain resolved networks that were distinct between diagnoses, an approach that may help identify molecular subtypes within diagnostic groups in the future. These networks included targets of rare and common variants across SCZ, ASD, ID and genes dysregulated in post-mortem brains of individuals with SCZ and BIP, as well as druggable targets such as *GRIN2A*. Convergent networks can model SCZ risk at the level of specific patients, potentially resolving molecular subtypes of SCZ and predicting precision therapeutics.

We prioritized and empirically tested three drugs predicted to reverse convergent signatures. *In vitro* validation revealed that *CALN1* activation blunted the normal effect of etomoxir, an inhibitor of fatty acid oxidation, on NGN2 neurons. While

this demonstrates opposing action of drug and SCZ-risk gene perturbations and suggests the utility of this approach for drug repurposing efforts, a major limitation is the lack of neuronal subtypes in the LINCs datasets used. Expanding large-scale perturbagen screenings to neuronal subtypes is crucial for drug-repurposing efforts within psychiatry. As the capacity to model polygenic risk using CRISPR-screens increases and perturbation-response signature catalogues expand to neuronal cell culture, convergent-network analysis may be able to resolve distinct molecular subtypes within diagnoses and aid in drug repurposing studies related to complex psychiatric disorders.

By coupling CRISPR-based perturbations to single-cell RNA sequencing of isogenic neuronal experiments, we not only increased the number of genes that can be queried, but likewise reduced experimental variation, altogether increasing our power to resolve convergence. However, there are limitations to this approach. First, it is necessary to test the generalizability of our findings beyond the set of ten genes chosen here; new CRISPRa and CRISPRi systems use different gRNA scaffold sequences[2,3], making new bi-directional, combinatorial gene perturbations in the same cell theoretically possible. Second, our CRISPRa analyses are from glutamatergic neurons only, and so do not consider the convergence across cell types or within more complex neuronal circuits. Finally, being most like fetal brain cells, hiPSC neurons cannot capture convergence that occurs at the time of symptom onset and thereafter; transcriptional consequences that may affect neurobiology during childhood or adolescence cannot be easily modelled with hiPSC-based platforms. Thus, future investigation to assess how transcriptional convergence differs across gene sets, drug/environmental contexts[71], brain regions[72] and cell types[73], developmental timespans[74], and donor backgrounds[75] will inform the cell-type-specific and context-dependent nature of convergence.

Given that our gene targets were prioritized based on the genetic and genomic evidence supporting their activation by SCZ-GWAS loci, it will be informative to revisit our findings across a larger number of genes and pathways, specifically considering whether manipulations made within or between biological pathways impact the convergence observed. Likewise, it would be interesting to repeat these studies in neural progenitor cells and/or over a developmental time-course. Intriguingly, although extensive evidence links ASD risk genes to both glutamatergic and GABAergic neurons[76], previously reported convergence of ASD genes impacts occurred in neural progenitor cells[24,27,28], impacting neurogenesis[24,27,28], WNT signaling[24] and gene expression[27]. A pressing question is thus the mechanisms by which convergence ultimately impacts synaptic activity, circuit function, and behavior. Improvement of CRISPR screening methods in co-culture and organoid systems would allow for studies in neurons at different stages of differentiation and maturity, making these inquiries more robust. Notably, here we included one pseudo-gene; given the unexpected phenotypic impact of its manipulation, and because multiple GWAS variants map to pseudo-genes, which may play critical roles in gene silencing and transcriptional regulation, it would be particularly interesting to explore the functional impact of these less well-explored genomic elements.

Our convergent genes are interesting to consider in the context of additive[16,77], epistatic[78], and omnigenic[18,70] models of inheritance. Do they represent "core genes" as conceptualized in the omnigenic model? Given our previous findings that there is emergent biology that results from combinatorial perturbation of SCZ risk genes beyond what would be expected from the additive effect of individually perturbed genes[30], and that these synergistic effects converge on synaptic function and psychiatric risk genes, an important next step will be to manipulate these risk genes alone and together. Our hope is that high-throughput combinatorial CRISPR-based perturbation methods will better resolve the complex genetic risk architecture of psychiatric disorders, including the convergent gene regulatory networks and/or the identity of peripheral master genes directing genetic risk.

Our findings support the hypothesis that common and rare psychiatric risk variants converge on the same biological pathways[30]. There is great value in continuing to explore as many rare and common risk loci as possible, agnostic to previously defined function, in a cell-type-specific and context-dependent manner. The translational impact of our work includes potential improvements to additive polygenic risk scores, prioritization of convergent genes for mechanistic follow-up, and identification of pathways that might serve as potential therapeutic targets. Overall, the as-yet unidentified regulatory nodes that lead to disruptions in synaptic function related to psychiatric endophenotypes represent exciting and unexplored therapeutic targets. Our overarching goal is to advance the field towards an era of precision medicine[79], whereby not just each patient's genetic variants, but also the expected interactions between them, can be used to predict symptom development, disorder trajectory, and potential therapeutic interventions.

MATERIALS AND METHODS

Prioritization of Seven SCZ eGene List: Day 7 hiPSC-derived NGN2-neuron library. eGenes are defined as genes with significant genetic regulation of gene expression levels. For prioritization, we used the Psychiatric Genomics Consortium (PGC3)-SCZ GWAS[2,80]. Transcriptomic imputation was performed with the EpiXcan[44] method utilizing the PsychENCODE transcriptome datasets of genotyped individuals[14] and epigenetic annotations from REMC[81] as previously described[82]; transcriptomes were imputed at the gene and isoform levels and features with training cross-validation $R^2 \geq 0.01$ were retained. The epigenetic imputation models were built with the PrediXcan[40] method (using a 50kbp window instead of 1Mbp for transcripts) utilizing the recently described ChIPseq datasets[46]; summary-level imputation was performed with S-PrediXcan[38]. Peaks were assigned to genes with the ChIPseeker R package[83]. Genes were ranked based on the association z-score for imputed gene expression. Genes that had no nominally associated imputed epigenetic activity ($p<0.01$) across the three different assays were not considered. Genes within the MHC were not considered. Six top coding genes and one top pseudo-gene were selected: *NEK4, PLCL1, UBE2Q2L, NAGA, FES, CALN1,* and *ZNF804.*

SCZ eGene Prioritization: Day 21 NPC-derived NGN2-neuron library. Transcriptomic imputation calculated using PrediXcan[40] from post-mortem CommonMind Consortium (CMC)[41] and PGC3-SCZ GWAS[3] data identified genes with significant ($p<6x10^{-6}$)[40] predicted differential expression between SCZ-cases and controls. Colocalization (using COLOC[37,42]) identified fine-mapped GWAS and eQTL associations with very strong evidence (PP4>0.8) of colocalization. The top significant SCZ eGenes identified by both analyses were prioritized. Any genes located in the major histocompatibility complex (MHC) locus were subsequently removed from the list. Ten top coding genes were selected: *CALN1*, *CLCN3, CUL9, DOC2A, PLCL1, INO8E0, SF3B1, SNAP91, TMEM219, ZNF823*. This list was intersected with the eGene set previously prioritized and functionally evaluated in hiPSC-neurons[30]; of the 108 SCZ-GWAS loci identified by the Psychiatric Genomics Consortium (PGC2)-SCZ GWAS[2,80], 19 were shown to harbor co-localized SCZ-GWAS and *cis*-eQTL (SNP–gene pairs within 1 Mb of a gene; COLOC PP4>0.8) signals in the CMC post-mortem brain RNA-Seq analysis of the Dorsa-Lateral Pre-Frontal Cortex (DLPFC)[41], five of which were predicted to involve only a single protein-coding gene, four were well-expressed in *NGN2*-neurons, and three were up-regulated in SCZ and could be robustly manipulated by CRISPRa: *SNAP91*, *TSNARE1*, and *CLCN3*. One functionally validated gRNA was included for each of these three genes[30].

Neuronal Differentiation of clonal hiPSCs. Clonal hiPSCs from two donors of European ancestry (#690 (XY) and #2607 (XY)) with lenti-EF1a-dCas9-VPR-Puro (Addgene #99373), pLV-TetO-hNGN2-eGFP-Neo, and lentiviral FUW-M2rtTA (Addgene #20342) were maintained in StemFlex™ Medium (ThermoFisher #A3349401) and passaged with EDTA (Life Technologies #15575-020).

On day 1, induction media (DMEM/F12 (ThermoFisher #10565,), 1× N2 (ThermoFisher #17502-048), 1× B27-RA (ThermoFisher #12587-010), 1× Antibiotic-Antimycotic (ThermoFisher #15240096), and 1 µg/mL doxycycline) was prepared and dispensed 2 mL of suspension at 1.2×10^6 cells/well in induction media onto a 6-well plate coated with matrigel (Corning #354230). On day 3, media is replaced with induction medium containing 1 µg/mL puromycin and 1 mg/mLG418. On day 5, split neurons were replated onto matrigel-coated plates and cells were dissociate with Accutase (Innovative Cell Technologies) for 5-10 min, washed with DMEM/10%FBS, gently resuspended, counted and centrifuged at 1,000×g for 5 min. The pellet was resuspended at a concentration of 1×10^6 cells/mL in neuron media [Brainphys (StemCell Technologies #05790), 1×N2 (ThermoFisher #17502-048), 1×B27-RA (ThermoFisher #12587-010), 1 mg/ml Natural Mouse Laminin (ThermoFisher #23017015), 20 ng/mL BDNF (Peprotech #450-02), 20 ng/mL GDNF (Peptrotech #450-10), 500 mg/mL Dibutyryl cyclic-AMP (Sigma #D0627), 200 nM L-ascorbic acid (Sigma #A0278)] with doxycycline, puromycin, G418 [4µM Ara-C (Sigma #C6645)] and 1×Thiazovivin (Sigma #420220). Cells were seeded 5×10^5 per 12-well plate. On day 7, neurons were harvested for scRNA sequencing.

NGN2-glutamatergic neuron induction of hiPSC-derived NPCs[32,33]. hiPSCs-derived NPCs were dissociated with Accutase Cell Detachment Solution (Innovative Cell Technologies, # AT-104), counted and transduced with rtTA (Addgene 20342) and *NGN2* (Addgene 99378) lentiviruses in StemFlex media containing 10 µM Thiazovivin (Millipore, #S1459). They were subsequently seeded at $1x10^6$ cells/well in the prepared 6-well plate. On day 1, medium was switched to non-viral induction medium (DMEM/F12 (Thermofisher, #10565018), 1% N-2 (Thermofisher, #17502048), 2% B-27-RA (Thermofisher, #12587010)) and doxycycline (dox) was added to each well at a final concentration of 1 µg/mL. At day 2, transduced hiPSCs were treated with 500 µg/mL G418 (Thermofisher, #10131035). At day 4, medium was replaced including 1 µg/mL dox and 4 µM cytosine arabinoside (Ara-C) to reduce the proliferation of non-neuronal cells. On day 5, young neurons were dissociated with Accutase Cell Detachment Solution (Innovative Cell Technologies, # AT-104), counted and seeded at a density of $1x10^6$ per well of a Matrigel-coated 12-well plate. Medium was switched to Brainphys neuron medium (Brainphys (STEMCELL, # 05790), 1% N-2, 2% B27-RA, 1 µg/mL Natural Mouse Laminin (Thermofisher, # 23017015), 10 ng/mL BDNF (R&D, #248), 10 ng/mL GDNF (R&D, #212), 500 µg/mL Dibutyryl cyclic-AMP (Sigma, #D0627), 200 nM L-ascorbic acid (Sigma, # A4403)). For seeding, 10 µM Thiazovivin (Millipore, #S1459), 500 µg/mL G418 and 4 µM Ara-C and 1 µg/mLdox were added. At day 6, medium was replaced with Brainphys neuron medium with 4 µM Ara-C and 1 µg/mL dox. Subsequently, 50% of the medium was replaced with fresh neuronal medium (lacking dox and Ara-C) once every other day until the neurons were harvested at day 21.

ECCITE-seq library generation. Expanded CRISPR-compatible CITE-seq (ECCITE-seq)[31], combines Cellular Indexing of Transcriptomes and Epitopes by sequencing (CITE-seq) and Cell Hashing for multiplexing and doublet detection[84] with direct detection of sgRNAs to enable single cell CRISPR screens with multi-modal single cell readout. By capturing pol III-expressed guide RNAs directly, this approach overcomes limitations of other single-cell CRISPR methods, which detect guide sequences by a proxy transcript, resulting in barcode switching and lower capture rates[85-87].

Neuronal ECCITE-seq. CRISPRa hiPSC *NGN2*-neurons (mid SCZ PRS control donors of European Ancestry 2607 (XY) and 690 (XY)) were transduced with the pooled gRNA at day -1. After maturation, 7-day-old *NGN2*-neurons were dissociated to single cell suspensions with papain, antibody-hashed[84], and bar-coded single cell cDNA generated using 10X Genomics Chromium[88]. NPC-derived NGN2-neurons (mid SCZ PRS control donors of European ancestry 2607 (XY) and 553 (XY)) were transduced with the mixed-pooled gRNA vectors (Addgene 99374) at day 17. At day 21, media was replaced by 0.5ml/well accutase containing 10 µm Rock inhibitor, THX (catalog no. 420220; Millipore) for 1 hour to dissociate neurons. Neurons were spun down (3 mins X 300g) and resuspended in DMEM/F12 + THX before proceeding to single cell sequencing.

Bioinformatics

Analysis of single-cell CRISPRa screens in DIV 7 and DIV 21 hiPSC-NGN2

Neurons. mRNA sequencing reads were mapped to the GRCh38 reference genome using the *Cellranger* Software. To generate count matrices for HTO and GDO libraries, the kallisto indexing and tag extraction (kite) workflow were used. Count matrices were used as input into the R/*Seurat* package[89] to perform downstream analyses, including QC, normalization, cell clustering, HTO/GDO demultiplexing, and DEG analysis[31,90]

Normalization and downstream analysis of RNA data were performed using the Seurat R package (v.2.3.0), which enables the integrated processing of multimodal single-cell datasets. Each ECCITE-seq experiment was initially processed separately. Cells with RNA UMI feature counts were filtered (200 < nFeature_RNA < 8000) and the percentage of all the counts belonging to the mitochondrial, ribosomal, and hemoglobin genes calculated using Seurat::PercentageFeatureSet. Hashtag and guide-tag raw counts were normalized using centered log ratio transformation, where counts were divided by the geometric mean of the corresponding tag across cells and log-transformed. For demultiplexing based on hashtag, Seurat::HTODemux function was used; and for guide-tag counts Seurat::MULTIseqDemux function within the Seurat package was performed with additional MULTIseq semi-supervised negative-cell reclassification. In both experiments, 8-10% of retained cells contained multiple gRNAs and were assigned as doublets after de-multiplexing. To remove variation related to cell-cycle phase of individual cells, cell cycle scores were assigned using Seurat::CellCycleScoring which uses a list of cell cycle markers[91] to segregate by markers of G2/M phase and markers of S phase. RNA UMI count data was then normalized, log-transformed and the percent mitochondrial, hemoglobulin, and ribosomal genes, batch, donor (HTO-maxID; as a biological replicate), cell cycle scores (Phase) regressed out using Seurat::SCTransform. The scaled residuals of this model represent a 'corrected' expression matrix, that was used for all downstream analyses. To ensure that cells assigned to a guide-tag identity class demonstrated successful perturbation of the target gene, we performed 'weighted-nearest neighbor' (WNN) analysis, to assign clusters based on both guide-tag identity class and gene expression. To identify successfully perturbed cells, we calculated a p-value based on the Wilcox rank sum test and Area Under the Curve (AUC) statistic, which reflects the power of each gene (or gRNA) to serve as a marker of a given cluster using Presto. WNN Clusters were then filtered based on two criteria (1) single gRNA-identity with an AUC statistic of >= 0.8 (where 1 means the gRNA is a perfect marker of a given cluster) and (2) a logFC >= 2 standard deviations of the mean or logFC > 0 and p-val > 0.05, of the target gene (but no other target genes) compared to scramble (non-targeting sgRNAs) controls. These clusters were then used for downstream analyses[92].

Meta-analysis of gene expression across perturbations. We performed a meta-analysis and heterogeneity test (METAL[93]) using the p-values and direction of effects (t-statistic), weighted according to sample size across all ten perturbations (Target vs. Scramble DEGs). Genes were assigned as convergent if they (1) had the same direction of effect across all ten targets, (2) had a META Bonferroni

adjusted p-value <= 0.05, and (3) had a heterogeneity Bonferroni adjusted p-value > 0.05 (**Supplemental Data 1**).

Cell Fraction Imputation and Quantification of NGN2 Cell culture Heterogeneity. Using CiberSortx, we imputed the cell-faction identity of randomly sampled scramble control cells from each experiment (n=100/exp) using the PsychEncode scRNAseq dataset as a reference (100 permutations). To determine if the level of heterogeneity of NGN2 maturity and subtype was similar between DIV7 and DIV21 *NGN2*-neurons in the given experiments, we performed a non-parametric Levene's Test for Homogeneity of Variance (LT-test) on the imputed cell fraction matrices.

Bayesian Bi-clustering to identify Target-Convergent Networks. Target-Convergent gene co-expression Networks (TCN) were built using an unsupervised Bayesian biclustering model, BicMix, on the log2cpm expression data from all the cells across 10 targets and Scramble gRNA jointly[94]. To account for neuronal maturity differences, expression matrices were batch corrected and normalized and the scramble cells from both experiments (matched scramble gRNA across experiments) used as a single control population. To perform this as a joint analysis across two experiments, (1) Count matrices from each experiment were combined and RNA transcripts, mitochondrial, ribosomal, and hemoglobin genes were removed (['^MT-|^RP[SL][[:digit:]]|^RPLP[[:digit:]]|^RPSA|^HB[ABDEGMQZ][[:digit:]]') as well as genes that had at fewer than 2 read counts in 90% of samples, (2) and limma:voom normalization and transformation was used to compute the log2cpm counts from the effective library sizes of each cell (16851 genes). We performed 40 runs of BicMix on these data and the output from iteration 400 of the variational Expectation-Maximization algorithm was used. The hyperparameters for BicMix were set based on previous extensive simulation studies[95]. Target-Convergent Network reconstruction[96] was performed to identify convergent networks across all possible combinations of 2,3,4,5,6,7 or 8 as well as all 10 of the targets (n=1003 combinations). For downstream gene enrichment analysis, network connections had to replicate in more than 10% of the runs with nodes with less than 5 edges and non-coding genes removed. Using FUMAGWAS: GENE2FUNC, the protein-coding genes were functionally annotated and overrepresentation gene-set analysis for each network gene set was performed[97]. Using WebGestalt (WEB-based Gene SeT AnaLysis Toolkit)[98], over-representation analysis (ORA) was performed on all convergent network gene sets against a curated list of common and rare variant target genes across ASD, BIP, SCZ, and ID[30].

Influence of Functional similarity on Convergence Degree. Functionally similarity scores across the eGenes represented in each set was calculated using three metrics: (1) GO Scores: the average semantic similarity score based on Gene Ontology pathway membership (within Biological Pathway (BP), Cellular Component (CC), and Molecular Function (MF) between genes in a set[56], (2) DLPFC score: based on the strength of the correlation in gene expression in the CMC (n=991 after QC) post-mortem dorsa-lateral pre-frontal cortex (DLPFC)

gene expression data, and (3) Signaling Score: based on the proportion of eGenes whose basic functional annotation was categorized as "signaling" (*CALN1, CLCN3, FES, NAGA, PLCL1, TMEM219*; with *PLCL1* and *CLCN3* further separated as specific synaptic genes) or four "epigenetic/regulatory" target genes (*SF3B1, UBE2Q2L, ZNF823, ZNF804A*; with *ZNF823, ZNF804A* as specific transcription factors*)* using FUMAGWAS: GENE2FUNC[97] (**Supplemental Fig. 7**).

Bi-clustering identifies co-expressed genes shared across the downstream transcriptomic impacts of any given set of eGene perturbations, thus, the resolved networks are the transcriptomic similarities between distinct perturbations (convergence)**.** While bi-clustering resolves convergent gene co-expression networks, the strength of convergence within a network can vary. We assigned each network a "degree of convergence" based on (1) network connectivity and (2) similarity of network genes based on biological pathway membership. We performed a principal components analysis on the functional similarity scores and the degree of network convergence. PCA loadings were used to determine to determine the effect of the included variables on the variability across sets (sets=1003, variables=6). To quantify this, we calculated two small world connectivity network coefficients: the cluster connectivity coefficient based on the proportion of edges present out of all possible edges (*Cp*) and the average path length (*Lp*)[99].

Here we define convergence as (1) increased connectivity of the resolved networks, and (2) functional similarity of genes within the network. Network connectivity was defined by the sum of the clustering coefficient (Cp) and the difference in average length path (Lp) from the maximum average length path resolved across all possible sets [(max)Lp-Lp]. Network functional similarity was scored by taking the sum of the mean semantic similarity scores between all genes in the network. Overall, convergence degree represented the sum of the network connectivity score and the network functional similarity score.

$$convergence = Cp + [\max(Lp) - Lp] + \sum_{1}^{N} MFsemsim + BPsemsim + CCsemsim$$

<u>*Convergent networks with matched patterns of gene expression in the post-mortem DLPFC.*</u> Target sets based on gene expression patterns in the CMC (n=991 after QC) post-mortem dorsa-lateral pre-frontal cortex (DLPFC). We performed K-means clustering to subset the data into 20 clusters based the Z-scored gene expression of the 10 target genes. Perturbation identities were assigned based on average positive Z-scores of >=0.5 within each cluster. We then assigned our single-cell data to clusters based on the overlap of perturbations and performed network reconstruction to replicate our convergent analysis using groups based on CMC post-mortem data. We retained clusters that resolved networks with at least 10% duplication rate and calculated convergence scores and performed GSEA using protein-coding network genes. Of the twenty clusters, networks were recovered for the combination of targets represented in cluster 4 (2 targets; 913 cells; 15% duplication; 13 node genes),

cluster 5 (3 targets; 1260 cells; 15% duplication; 13 node genes), cluster 6 (6 targets; 2035 cells; 15% duplication; 34 node genes), cluster 9 (6 targets, 1822 cells, 20% duplication, 108 node genes), cluster 11 (5 targets; 1640 cells; 15% duplication; 25 node genes), cluster 12 (6 targets; 2357 cells; 20% duplication, 152 node genes), cluster 13 (5 targets; 1741 cells; 17.5% duplication, 17 node genes), cluster 18 (6 targets; 1884 cells, 15% duplication, 25 nodes), cluster 19 (6 targets, 2327 cells, 20% duplication, 153 nodes), cluster 20 (6 targets, 2015 cells, 20% duplication, 33 nodes), while low confidence convergence was resolved for cluster 1 (5 targets, 1600 cells; 7.5% duplication; 38 node genes), cluster 8 (3 targets, 1233 cells, 7.5% duplication, 38 node genes), cluster 14 (3 targets, 1020 cells, 5% duplication, 23 nodes) and 16 (4 targets, 1177 cells, 2.5% duplication, 16 nodes). To determine if convergent networks were distinct between diagnostic groups, we first performed a Pearson's chi-squared test to determine whether there was a significant difference between the expected frequencies and the observed frequencies in diagnosis of AFF, BIP and SCZ within the clusters and then calculated Jaccard Similarity Indices between clusters based on convergent network gene membership.

Drug prioritization based on perturbation signature reversal in LiNCs Neuronal Cell Lines: To identify drugs that could reverse the resolved convergent perturbation signature across all ten targets, and within each target individually, we used the Query tool from The Broad Institute's Connectivity Map (Cmap) Server. Briefly, the tool computes weighted enrichment scores (WTCS) between the query set and each signature in the Cmap LINCs gene expression data (dose, time, drug, cell-line), normalizes the WRCS by dividing by signed mean w/in each perturbation (NCS), and computes FDR as fraction of "null signatures" (DMSO) where the absolute NCS exceeds reference signature[100]. We prioritized drugs that reversed signatures specifically in neuronal cells (either neurons (NEU) of neural progenitor cells (NPCs) with NCS <= -1.00) and filtered for (i) drugs that cross the blood-brain barriers, (ii) drugs that target genes expressed in hiPSC-derived NGN2-neurons based on bulk RNA-sequencing data from our lab and (ii) drugs that are currently launched or in clinical trial according the cMAP Drug Repurposing database and without evidence of neurotoxicity.

Neurite analysis: Day 7 iGLUTs were seeded as $1.5x10^4$ cells/well in a 96-well plate coated with 4x Matrigel at day 3. iGLUTs were plated in media containing individual target gRNA vectors (Addgene 99374), either targeting CALN1 or TMEM219 eGenes or scramble controls. Medium was switched to non-viral medium four hours post infection. At day 4, transduced iGLUTs were treated with corresponding antibiotics to the gRNA lentiviruses (1 mg/ml HygroB for lentiguide-Hygro/lentiguide-Hygro-mTagBFP2) followed by half medium changes until the neurons were fixed at day 7 (**Supplemental Fig. 1E**). At day 5, cells were treated for 48hrs with either Anandamide (10µM), Etomoxir (10µM), Somatostatin (10µM), or matched vehicles. Following drug treatment, cultures were fixed using 4% formaldehyde/sucrose in PBS with Ca^{2+} and Mg^{2+} for 10 minutes at room temperature (RT). Fixed cultures were washed twice in PBS and permeabilized and blocked using 0.1% Triton/2% Normal Donkey Serum (NDS) in PBS for two hours. Cultures were then incubated with primary antibody

solution (1:1000 MAP2 anti chicken (Abcam, ab5392) in PBS with 2% NDS) overnight at 4°C. Cultures were then washed 3x with PBS and incubated with secondary antibody solution (1:500 donkey anti chicken Alexa 647 (Life technologies, A10042) in PBS with 2% NDS) for 1 hour at RT. Cultures were washed a further 3x with PBS with the second wash containing 1 µg/ml DAPI. Fixed cultures were then imaged on a CellInsight CX7 HCS Platform with a 20x objective (0.4 NA) and neurite tracing analysis performed using the neurite tracing module in the Thermo Scientific HCS Studio 4.0 Cell Analysis Software. 12 wells were imaged per condition across a minimum 2 independent cell lines, with 9 images acquired per well for neurite tracing analysis. A one-way ANOVA with a post hoc Bonferroni multiple comparisons test was performed on data for neurite length per neuron using Graphpad Prism.

Synapse analyses: Commercially available primary human astrocytes (pHAs, Sciencell, #1800; isolated from fetal female brain) were seeded on D3 at 1.7×10^4 cells per well on a 4x Matrigel-coated 96□W plate in neuronal media supplemented with 2% fetal bovine serum (FBS). iGLUTs were seeded over the astrocyte monolayer as 1.5×10^5 cells/well at day 5 post induction. Half changes of neuronal media were performed twice a week until fixation. At day 13, iGLUTs were treated with 200 nM Ara-C to reduce the proliferation of non-neuronal cells in the culture. At day 18, Ara-C was completely withdrawn by full medium change while adding media containing CALN1, TMEM219, or scramble gRNA vectors. Medium was switched to non-viral medium four hours post infection. At day 19, transduced iGLUTs were treated with corresponding antibiotics to the gRNA lentiviruses (1 mg/ml HygroB for lentiguide-Hygro/lentiguide-Hygro-mTagBFP2) followed by half medium changes until the neurons were fixed at day 21 (**Supplemental Fig. 1E**). At day 21, cells were treated for 48hrs with either Anandamide (10µM), Etomoxir (10µM), Somatostatin (10µM), or matched vehicles. Following drug treatment, cultures were fixed and immunostained as described previously, with an additional antibody stain for Synapsin1 (primary antibody: 1:500 Synapsin1 anti mouse (Synaptic Systems, 106 011); secondary antibody: donkey anti mouse Alexa 568 (Life technologies A10037)). Stained cultures were imaged and analysed as above using the synaptogenesis module in the Thermo Scientific HCS Studio 4.0 Cell Analysis Software to determine SYN1+ puncta number, area and intensity per neurite length in each image. 20 wells were imaged per condition across a minimum of 2 independent cell lines, with 9 images acquired per well for synaptic puncta analysis. A one-way ANOVA with a post hoc Bonferroni multiple comparisons test was performed on data for puncta number per neurite length using Graphpad Prism.

Antibody	Species	Supplier	Product number	Dilution

MAP2	Ck	Abcam	ab5392	1:500
SYNAPSIN1	Ms	Synaptic Systems	106 011	1:500
Alexa 568 anti-Mouse	Ms	Life technologies	A10037	1:500
Alexa 647 anti-Chicken	Ck	Life technologies	A10042	1:500

Multiple Electrode array (MEA)

Commercially available primary human astrocytes (pHAs, Sciencell, #1800; isolated from fetal female brain) were seeded on D3 at $1.7x10^4$ cells per well on a 4x Matrigel-coated 48□W MEA plate (catalog no. M768-tMEA-48W; Axion Biosystems) in neuronal media supplemented with 2% fetal bovine serum (FBS). At D5, iGLUTs were detached, spun down and seeded on the pHA cultures at $1.5x10^5$ cells per well. Half changes of neuronal media supplemented with 2% FBS were performed twice a week until day 42. At day 13, co-cultures were treated with 200 nM Ara-C to reduce the proliferation of non-neuronal cells in the culture. At Day 18, Ara-C was completely withdrawn by full medium change. At day 25, a full media change was performed to add media containing CALN1, TMEM219, or scramble gRNA vectors either targeting eGenes or scramble controls. Medium was switched to non-viral medium four hours post infection. At day 26, cells were treated for 48hrs with either Anandamide (10µM), Etomoxir (10µM), Somatostatin (10µM), or matched vehicles. Following drug treatment, electrical activity of iGLUTs was recorded at 37°C using the Axion Maestro MEA reader (Axion Biosystems) (**Supplemental Fig. 1E**). Recording was performed via AxiS 2.4. Batch mode/statistic compiler tool was run following the final recording. Quantitative analysis of the recording was exported as Microsoft excel sheet. Data from 6-12 biological replicates were analyzed using GraphPad PRISM 6 software or R.

STATEMENT OF ETHICS

Ethical approval was not required because the hiPSC lines, lacking association with any identifying information and widely accessible from a public repository, are thus not considered to be human subjects research. Post-mortem DLPFC data are similarly lacking identifiable information and are not considered human subjects research.

CONFLICT OF INTEREST STATEMENT

The authors declare no conflicts of interest.

FUNDING SOURCES

This work was supported by F31MH130122 (K.G.T), R01MH109897 (K.J.B., P.R.), R56MH101454 (K.J.B., E.S., L.H.), R01MH123155 (K.J.B.) and R01ES033630 (L.H., K.J.B.), R01MH124839 (LMH), R01MH118278 (LMH). K08MH122911 (G.V.). R01MH125246 (PR), U01MH116442 (PR), R01MH109677 (PR), I01BX002395 (PR).

AUTHOR CONTRIBUTIONS

SCZ eGene lists were prioritized by E.S., L.H., W.Z., G.V. and P.R, together with K.J.B. Epigenome data provided by K.G., S.A. and P.R. The ECCITE-seq pipeline was adapted to hiPSC-neurons by A.L., supported by P.J.M.D., J.F., A.Y. and S.C. ECCITE-seq *NGN2*-neuronal studies were conducted by A.L. and P.J.M.D. 10x analyses were conducted by J.F, and preliminary ECCITE-seq quality control conducted by MW. Convergent analyses were conceptualized by K.J.B. and L.H., developed and conducted entirely by K.G.T. The paper was written by K.G.T., L.H. and K.J.B., with input from all authors.

Special thanks to Michael Talkowski and Douglas Ruderfer for countless discussions on convergence.

DATA AND CODE AVAILABILITY

All source donor hiPSCs have been deposited at the Rutgers University Cell and DNA Repository (study 160; http://www.nimhstemcells.org/); dCas9-VPR hiPSCs are in the process of being submitted in advance of publication.

The accession number for sc-RNA sequencing data reported in this paper is Gene expression omnibus (GEO):GSE200774. Processed data and accompanying code can be accessed through Synapse (syn27819129)

REFERENCES

1 Schizophrenia Working Group of the Psychiatric Genomics, C. *et al.* Biological insights from 108 schizophrenia-associated genetic loci. *Nature* **511**, 421-427, doi:10.1038/nature13595 (2014).

2 Pardinas, A. F. *et al.* Common schizophrenia alleles are enriched in mutation-intolerant genes and in regions under strong background selection. *Nat Genet*, doi:10.1038/s41588-018-0059-2 (2018).

3 Trubetskoy, V. *et al.* Mapping genomic loci implicates genes and synaptic biology in schizophrenia. *Nature* **604**, 502-508, doi:10.1038/s41586-022-04434-5 (2022).

4 Finucane, H. K. *et al.* Heritability enrichment of specifically expressed genes identifies disease-relevant tissues and cell types. *Nat Genet* **50**, 621-629, doi:10.1038/s41588-018-0081-4 (2018).

5 Skene, N. G. *et al.* Genetic identification of brain cell types underlying schizophrenia. *Nat Genet* **50**, 825-833, doi:10.1038/s41588-018-0129-5 (2018).

6 Jaffe, A. E. *et al.* Developmental and genetic regulation of the human cortex transcriptome illuminate schizophrenia pathogenesis. *Nat Neurosci* **21**, 1117-1125, doi:10.1038/s41593-018-0197-y (2018).

7 Hall, L. S. *et al.* A transcriptome-wide association study implicates specific pre- and post-synaptic abnormalities in schizophrenia. *Hum Mol Genet* **29**, 159-167, doi:10.1093/hmg/ddz253 (2020).

8 Gulsuner, S. *et al.* Spatial and temporal mapping of de novo mutations in schizophrenia to a fetal prefrontal cortical network. *Cell* **154**, 518-529, doi:10.1016/j.cell.2013.06.049 (2013).

9 Schork, A. J. *et al.* A genome-wide association study of shared risk across psychiatric disorders implicates gene regulation during fetal

neurodevelopment. *Nat Neurosci* **22**, 353-361, doi:10.1038/s41593-018-0320-0 (2019).

10 Radulescu, E. *et al.* Identification and prioritization of gene sets associated with schizophrenia risk by co-expression network analysis in human brain. *Mol Psychiatry*, doi:10.1038/s41380-018-0304-1 (2018).

11 Rajarajan, P. *et al.* Neuron-specific signatures in the chromosomal connectome associated with schizophrenia risk. *Science* **362**, doi:10.1126/science.aat4311 (2018).

12 Li, J. *et al.* Spatiotemporal profile of postsynaptic interactomes integrates components of complex brain disorders. *Nat Neurosci* **20**, 1150-1161, doi:10.1038/nn.4594 (2017).

13 Jia, P., Chen, X., Fanous, A. H. & Zhao, Z. Convergent roles of de novo mutations and common variants in schizophrenia in tissue-specific and spatiotemporal co-expression network. *Translational psychiatry* **8**, 105, doi:10.1038/s41398-018-0154-2 (2018).

14 Gandal, M. J. *et al.* Transcriptome-wide isoform-level dysregulation in ASD, schizophrenia, and bipolar disorder. *Science* **362**, doi:10.1126/science.aat8127 (2018).

15 Gandal, M. J. *et al.* Shared molecular neuropathology across major psychiatric disorders parallels polygenic overlap. *Science* **359**, 693-697, doi:10.1126/science.aad6469 (2018).

16 Wainschtein, P. *et al.* Recovery of trait heritability from whole genome sequence data. *bioRxiv*, 588020, doi:10.1101/588020 (2019).

17 Nag, A., McCarthy, M. I. & Mahajan, A. Large-Scale Analyses Provide No Evidence For Gene-Gene Interactions Influencing Type 2 Diabetes Risk. *Diabetes*, doi:10.2337/db20-0224 (2020).

18 Liu, X., Li, Y. I. & Pritchard, J. K. Trans Effects on Gene Expression Can Drive Omnigenic Inheritance. *Cell* **177**, 1022-1034 e1026, doi:10.1016/j.cell.2019.04.014 (2019).

19 Hess, J. L. *et al.* A polygenic resilience score moderates the genetic risk for schizophrenia. *Mol Psychiatry*, doi:10.1038/s41380-019-0463-8 (2019).

20 Yi, F. *et al.* Autism-associated SHANK3 haploinsufficiency causes Ih channelopathy in human neurons. *Science* **352**, aaf2669, doi:10.1126/science.aaf2669 (2016).

21 Pak, C. *et al.* Human Neuropsychiatric Disease Modeling using Conditional Deletion Reveals Synaptic Transmission Defects Caused by Heterozygous Mutations in NRXN1. *Cell stem cell* **17**, 316-328, doi:10.1016/j.stem.2015.07.017 (2015).

22 Deneault, E. *et al.* Complete Disruption of Autism-Susceptibility Genes by Gene Editing Predominantly Reduces Functional Connectivity of Isogenic Human Neurons. *Stem Cell Reports* **11**, 1211-1225, doi:10.1016/j.stemcr.2018.10.003 (2018).

23 Srikanth, P. *et al.* Genomic DISC1 Disruption in hiPSCs Alters Wnt Signaling and Neural Cell Fate. *Cell reports* **12**, 1414-1429, doi:10.1016/j.celrep.2015.07.061 (2015).

24 Cederquist, G. Y. *et al.* A Multiplex Human Pluripotent Stem Cell Platform Defines Molecular and Functional Subclasses of Autism-Related Genes. *Cell stem cell* **27**, 35-49 e36, doi:10.1016/j.stem.2020.06.004 (2020).
25 Paulsen, B. *et al.* Autism genes converge on asynchronous development of shared neuron classes. *Nature* **602**, 268-273, doi:10.1038/s41586-021-04358-6 (2022).
26 Li, C. *et al.* Single-cell brain organoid screening identifies developmental defects in autism. *bioRxiv*, 2022.2009.2015.508118, doi:10.1101/2022.09.15.508118 (2022).
27 Jin, X. *et al.* In vivo Perturb-Seq reveals neuronal and glial abnormalities associated with autism risk genes. *Science* **370**, doi:10.1126/science.aaz6063 (2020).
28 Willsey, H. R. *et al.* Parallel in vivo analysis of large-effect autism genes implicates cortical neurogenesis and estrogen in risk and resilence. *Neuron* (2021).
29 Singh, T. *et al.* Rare coding variants in ten genes confer substantial risk for schizophrenia. *Nature* **604**, 509-516, doi:10.1038/s41586-022-04556-w (2022).
30 Schrode, N. *et al.* Synergistic effects of common schizophrenia risk variants. *Nat Genet* **51**, 1475-1485, doi:10.1038/s41588-019-0497-5 (2019).
31 Mimitou, E. P. *et al.* Multiplexed detection of proteins, transcriptomes, clonotypes and CRISPR perturbations in single cells. *Nat Methods* **16**, 409-412, doi:10.1038/s41592-019-0392-0 (2019).
32 Zhang, Y. *et al.* Rapid single-step induction of functional neurons from human pluripotent stem cells. *Neuron* **78**, 785-798, doi:10.1016/j.neuron.2013.05.029 (2013).
33 Ho, S. M. *et al.* Rapid Ngn2-induction of excitatory neurons from hiPSC-derived neural progenitor cells. *Methods* **101**, 113-124, doi:10.1016/j.ymeth.2015.11.019 (2016).
34 Roussos, P. *et al.* A role for noncoding variation in schizophrenia. *Cell reports* **9**, 1417-1429, doi:10.1016/j.celrep.2014.10.015 (2014).
35 Hauberg, M. E. *et al.* Large-Scale Identification of Common Trait and Disease Variants Affecting Gene Expression. *Am J Hum Genet* **101**, 157, doi:10.1016/j.ajhg.2017.06.003 (2017).
36 Hauberg, M. E. *et al.* Differential activity of transcribed enhancers in the prefrontal cortex of 537 cases with schizophrenia and controls. *Mol Psychiatry*, doi:10.1038/s41380-018-0059-8 (2018).
37 Dobbyn, A. *et al.* Landscape of Conditional eQTL in Dorsolateral Prefrontal Cortex and Co-localization with Schizophrenia GWAS. *Am J Hum Genet* **102**, 1169-1184, doi:10.1016/j.ajhg.2018.04.011 (2018).
38 Barbeira, A. N. *et al.* Exploring the phenotypic consequences of tissue specific gene expression variation inferred from GWAS summary statistics. *Nat Commun* **9**, 1825, doi:10.1038/s41467-018-03621-1 (2018).

39 Gusev, A. *et al.* Transcriptome-wide association study of schizophrenia and chromatin activity yields mechanistic disease insights. *Nat Genet* **50**, 538-548, doi:10.1038/s41588-018-0092-1 (2018).
40 Huckins, L. M. *et al.* Gene expression imputation across multiple brain regions provides insights into schizophrenia risk. *Nat Genet* **51**, 659-674, doi:10.1038/s41588-019-0364-4 (2019).
41 Fromer, M. *et al.* Gene expression elucidates functional impact of polygenic risk for schizophrenia. *Nat Neurosci* **19**, 1442-1453, doi:10.1038/nn.4399 (2016).
42 Giambartolomei, C. *et al.* Bayesian test for colocalisation between pairs of genetic association studies using summary statistics. *PLoS genetics* **10**, e1004383, doi:10.1371/journal.pgen.1004383 (2014).
43 Wang, D. *et al.* Comprehensive functional genomic resource and integrative model for the human brain. *Science* **362**, doi:10.1126/science.aat8464 (2018).
44 Zhang, W. *et al.* Integrative transcriptome imputation reveals tissue-specific and shared biological mechanisms mediating susceptibility to complex traits. *Nat Commun* **10**, 3834, doi:10.1038/s41467-019-11874-7 (2019).
45 Cao, C. *et al.* Power analysis of transcriptome-wide association study: Implications for practical protocol choice. *PLoS genetics* **17**, e1009405, doi:10.1371/journal.pgen.1009405 (2021).
46 Girdhar, K. *et al.* Chromatin domain alterations linked to 3D genome organization in a large cohort of schizophrenia and bipolar disorder brains. *Nat Neurosci* **25**, 474-483, doi:10.1038/s41593-022-01032-6 (2022).
47 Chavez, A. *et al.* Highly efficient Cas9-mediated transcriptional programming. *Nat Methods* **12**, 326-328, doi:10.1038/nmeth.3312 (2015).
48 Chavez, A. *et al.* Comparison of Cas9 activators in multiple species. *Nat Methods* **13**, 563-567, doi:10.1038/nmeth.3871 (2016).
49 Ho, S. M. *et al.* Evaluating Synthetic Activation and Repression of Neuropsychiatric-Related Genes in hiPSC-Derived NPCs, Neurons, and Astrocytes. *Stem Cell Reports*, doi:10.1016/j.stemcr.2017.06.012 (2017).
50 Lin, H. C. *et al.* NGN2 induces diverse neuron types from human pluripotency. *Stem Cell Reports* **16**, 2118-2127, doi:10.1016/j.stemcr.2021.07.006 (2021).
51 Lobentanzer, S., Hanin, G., Klein, J. & Soreq, H. Integrative Transcriptomics Reveals Sexually Dimorphic Control of the Cholinergic/Neurokine Interface in Schizophrenia and Bipolar Disorder. *Cell reports* **29**, 764-777 e765, doi:10.1016/j.celrep.2019.09.017 (2019).
52 Kipanyula, M. J., Kimaro, W. H. & Seke Etet, P. F. The Emerging Roles of the Calcineurin-Nuclear Factor of Activated T-Lymphocytes Pathway in Nervous System Functions and Diseases. *J Aging Res* **2016**, 5081021, doi:10.1155/2016/5081021 (2016).
53 Torretta, S. *et al.* NURR1 and ERR1 Modulate the Expression of Genes of a DRD2 Coexpression Network Enriched for Schizophrenia Risk. *J Neurosci* **40**, 932-941, doi:10.1523/JNEUROSCI.0786-19.2019 (2020).

54 Batiuk, M. Y. *et al.* Upper cortical layer-driven network impairment in schizophrenia. *Sci Adv* **8**, eabn8367, doi:10.1126/sciadv.abn8367 (2022).
55 Teixeira, J. R., Szeto, R. A., Carvalho, V. M. A., Muotri, A. R. & Papes, F. Transcription factor 4 and its association with psychiatric disorders. *Translational psychiatry* **11**, 19, doi:10.1038/s41398-020-01138-0 (2021).
56 Yu, G. Gene Ontology Semantic Similarity Analysis Using GOSemSim. *Methods in molecular biology* **2117**, 207-215, doi:10.1007/978-1-0716-0301-7_11 (2020).
57 Childers, E., Bowen, E. F. W., Rhodes, C. H. & Granger, R. Immune-Related Genomic Schizophrenic Subtyping Identified in DLPFC Transcriptome. *Genes (Basel)* **13**, doi:10.3390/genes13071200 (2022).
58 Luo, C. *et al.* Subtypes of schizophrenia identified by multi-omic measures associated with dysregulated immune function. *Mol Psychiatry* **26**, 6926-6936, doi:10.1038/s41380-021-01308-6 (2021).
59 Li, Z. *et al.* Identification of potential biomarkers and their correlation with immune infiltration cells in schizophrenia using combinative bioinformatics strategy. *Psychiatry Res* **314**, 114658, doi:10.1016/j.psychres.2022.114658 (2022).
60 Zubiaur, P. *et al.* Variants in COMT, CYP3A5, CYP2B6, and ABCG2 Alter Quetiapine Pharmacokinetics. *Pharmaceutics* **13**, doi:10.3390/pharmaceutics13101573 (2021).
61 Corsello, S. M. *et al.* The Drug Repurposing Hub: a next-generation drug library and information resource. *Nat Med* **23**, 405-408, doi:10.1038/nm.4306 (2017).
62 Kurita, M. *et al.* HDAC2 regulates atypical antipsychotic responses through the modulation of mGlu2 promoter activity. *Nat Neurosci* **15**, 1245-1254, doi:10.1038/nn.3181 (2012).
63 Lichtstein, D. *et al.* Na(+), K(+)-ATPase Signaling and Bipolar Disorder. *Int J Mol Sci* **19**, doi:10.3390/ijms19082314 (2018).
64 Rees, E. *et al.* Targeted Sequencing of 10,198 Samples Confirms Abnormalities in Neuronal Activity and Implicates Voltage-Gated Sodium Channels in Schizophrenia Pathogenesis. *Biol Psychiatry* **85**, 554-562, doi:10.1016/j.biopsych.2018.08.022 (2019).
65 Zuccoli, G. S., Brandao-Teles, C., Vieira, G. M., Gomes, F. V. & Crunfli, F. Molecular Findings Guiding the Modulation of the Endocannabinoid System as a Potential Target to Treat Schizophrenia. *Adv Exp Med Biol* **1400**, 89-103, doi:10.1007/978-3-030-97182-3_7 (2022).
66 Leweke, F. M. *et al.* Cannabidiol and Amisulpride Improve Cognition in Acute Schizophrenia in an Explorative, Double-Blind, Active-Controlled, Randomized Clinical Trial. *Frontiers in pharmacology* **12**, 614811, doi:10.3389/fphar.2021.614811 (2021).
67 Shen, H. *et al.* Adjunctive therapy with statins in schizophrenia patients: A meta-analysis and implications. *Psychiatry Res* **262**, 84-93, doi:10.1016/j.psychres.2018.02.018 (2018).
68 Sommer, I. E. *et al.* Simvastatin Augmentation for Patients With Early-Phase Schizophrenia-Spectrum Disorders: A Double-Blind, Randomized

Placebo-Controlled Trial. *Schizophr Bull* **47**, 1108-1115, doi:10.1093/schbul/sbab010 (2021).

69 Cao, B., Chen, Y., McIntyre, R. S. & Yan, L. Acyl-Carnitine plasma levels and their association with metabolic syndrome in individuals with schizophrenia. *Psychiatry Res* **293**, 113458, doi:10.1016/j.psychres.2020.113458 (2020).

70 Boyle, E. A., Li, Y. I. & Pritchard, J. K. An Expanded View of Complex Traits: From Polygenic to Omnigenic. *Cell* **169**, 1177-1186, doi:10.1016/j.cell.2017.05.038 (2017).

71 Seah, C. *et al.* Modeling gene x environment interactions in PTSD using human neurons reveals diagnosis-specific glucocorticoid-induced gene expression. *Nat Neurosci* **25**, 1434-1445, doi:10.1038/s41593-022-01161-y (2022).

72 Sieberts, S. K. *et al.* Large eQTL meta-analysis reveals differing patterns between cerebral cortical and cerebellar brain regions. *Sci Data* **7**, 340, doi:10.1038/s41597-020-00642-8 (2020).

73 Bryois, J. *et al.* Cell-type specific cis-eQTLs in eight brain cell-types identifies novel risk genes for human brain disorders. *medRxiv*, 2021.2010.2009.21264604, doi:10.1101/2021.10.09.21264604 (2021).

74 Walker, R. L. *et al.* Genetic Control of Expression and Splicing in Developing Human Brain Informs Disease Mechanisms. *Cell* **179**, 750-771 e722, doi:10.1016/j.cell.2019.09.021 (2019).

75 Dobrindt, K. *et al.* Publicly Available hiPSC Lines with Extreme Polygenic Risk Scores for Modeling Schizophrenia. *Complex Psychiatry* **6**, 68–82, doi:10.1159/000512716 (2020).

76 Satterstrom, F. K. *et al.* Large-Scale Exome Sequencing Study Implicates Both Developmental and Functional Changes in the Neurobiology of Autism. *Cell* **180**, 568-584 e523, doi:10.1016/j.cell.2019.12.036 (2020).

77 Wray, N. R., Wijmenga, C., Sullivan, P. F., Yang, J. & Visscher, P. M. Common Disease Is More Complex Than Implied by the Core Gene Omnigenic Model. *Cell* **173**, 1573-1580, doi:10.1016/j.cell.2018.05.051 (2018).

78 Zuk, O., Hechter, E., Sunyaev, S. R. & Lander, E. S. The mystery of missing heritability: Genetic interactions create phantom heritability. *Proc Natl Acad Sci U S A* **109**, 1193-1198, doi:10.1073/pnas.1119675109 (2012).

79 McMahon, F. J. & Insel, T. R. Pharmacogenomics and personalized medicine in neuropsychiatry. *Neuron* **74**, 773-776, doi:10.1016/j.neuron.2012.05.004 (2012).

80 Schizophrenia Working Group of the Psychiatric Genomics Consortium. Biological insights from 108 schizophrenia-associated genetic loci. *Nature* **511**, 421-427, doi:10.1038/nature13595 (2014).

81 Roadmap Epigenomics, C. *et al.* Integrative analysis of 111 reference human epigenomes. *Nature* **518**, 317-330, doi:10.1038/nature14248 (2015).

82 Fullard, J. F. *et al.* Single-nucleus transcriptome analysis of human brain immune response in patients with severe COVID-19. *Genome Med* **13**, 118, doi:10.1186/s13073-021-00933-8 (2021).

83 Yu, G., Wang, L. G. & He, Q. Y. ChIPseeker: an R/Bioconductor package for ChIP peak annotation, comparison and visualization. *Bioinformatics* **31**, 2382-2383, doi:10.1093/bioinformatics/btv145 (2015).

84 Stoeckius, M. *et al.* Cell Hashing with barcoded antibodies enables multiplexing and doublet detection for single cell genomics. *Genome biology* **19**, 224, doi:10.1186/s13059-018-1603-1 (2018).

85 Dixit, A. *et al.* Perturb-Seq: Dissecting Molecular Circuits with Scalable Single-Cell RNA Profiling of Pooled Genetic Screens. *Cell* **167**, 1853-1866 e1817, doi:10.1016/j.cell.2016.11.038 (2016).

86 Adamson, B. *et al.* A Multiplexed Single-Cell CRISPR Screening Platform Enables Systematic Dissection of the Unfolded Protein Response. *Cell* **167**, 1867-1882 e1821, doi:10.1016/j.cell.2016.11.048 (2016).

87 Datlinger, P. *et al.* Pooled CRISPR screening with single-cell transcriptome readout. *Nat Methods* **14**, 297-301, doi:10.1038/nmeth.4177 (2017).

88 Zheng, G. X. *et al.* Massively parallel digital transcriptional profiling of single cells. *Nat Commun* **8**, 14049, doi:10.1038/ncomms14049 (2017).

89 Butler, A., Hoffman, P., Smibert, P., Papalexi, E. & Satija, R. Integrating single-cell transcriptomic data across different conditions, technologies, and species. *Nature Biotechnology* **36**, 411, doi:10.1038/nbt.4096 (2018).

90 Papalexi, E. *et al.* Characterizing the molecular regulation of inhibitory immune checkpoints with multimodal single-cell screens. *Nature Genetics* **53**, 322-331, doi:10.1038/s41588-021-00778-2 (2021).

91 Tirosh, I. *et al.* Dissecting the multicellular ecosystem of metastatic melanoma by single-cell RNA-seq. *Science* **352**, 189-196, doi:10.1126/science.aad0501 (2016).

92 Tian, R. *et al.* CRISPR Interference-Based Platform for Multimodal Genetic Screens in Human iPSC-Derived Neurons. *Neuron*, doi:10.1016/j.neuron.2019.07.014 (2019).

93 Willer, C. J., Li, Y. & Abecasis, G. R. METAL: fast and efficient meta-analysis of genomewide association scans. *Bioinformatics* **26**, 2190-2191, doi:10.1093/bioinformatics/btq340 (2010).

94 Gao, C., McDowell, I. C., Zhao, S., Brown, C. D. & Engelhardt, B. E. Context Specific and Differential Gene Co-expression Networks via Bayesian Biclustering. *PLoS Comput Biol* **12**, e1004791, doi:10.1371/journal.pcbi.1004791 (2016).

95 Gao C, B. C., Engelhardt BE. A latent factor model with a mixture of sparse and dense factors to model gene expression data with confounding effects. *arXiv* (2013).

96 Saha, A. *et al.* Co-expression networks reveal the tissue-specific regulation of transcription and splicing. *Genome Res* **27**, 1843-1858, doi:10.1101/gr.216721.116 (2017).

97 Watanabe, K., Taskesen, E., van Bochoven, A. & Posthuma, D. Functional mapping and annotation of genetic associations with FUMA. *Nat Commun* **8**, 1826, doi:10.1038/s41467-017-01261-5 (2017).

98 Wang, J. & Liao, Y. *WebGestaltR: Gene Set Analysis Toolkit WebGestaltR. R package version 0.4.3.*, <https://CRAN.R-project.org/package=WebGestaltR> (2020).

99 Watts, D. J. & Strogatz, S. H. Collective dynamics of 'small-world' networks. *Nature* **393**, 440-442, doi:10.1038/30918 (1998).

100 Subramanian, A. *et al.* A Next Generation Connectivity Map: L1000 Platform and the First 1,000,000 Profiles. *Cell* **171**, 1437-1452 e1417, doi:10.1016/j.cell.2017.10.049 (2017).

Table 1. SCZ-GWAS loci with strong evidence for eQTL mechanisms. PGC3 SCZ-GWAS genes prioritized as epigenetic/regulatory (blue) and signalling (red) for pathway studies.

GWAS						COLOC	PrediXcan		hiPSC-neuron expression		
Chr	**SNP**	**P**	**LD range**	**Gene**	**Annotated Function**	**PP4**	**z**	**P**	**iGLU (RPKM)**	**iGABA (FPKM)**	**iDOPA (FPKM)**
19	rs72986630	3.07E-10	10832225…12839819	***ZNF823***	epigenetic	0.999253	6.350252	2.15E-10	4.0	2.2	5.4
6	rs113113059	2.29E-11	42150013…44192158	***CUL9***	ubiquitination	0.953677	5.754229	8.70E-09	4.0	9.5	23.2
7	rs2944821	1.90E-09	70244499…72912040	***CALN1***	calcium signaling	0.913966	5.547481	2.90E-08	0.9	3.1	0.9
16	rs3814883	8.82E-15	29007489…31016970	***INO80E***	epigenetic	0.894347	7.639276	2.18E-14	6.2	55.0	41.0
6	rs2022265	3.74E-10	83262613…85419243	***SNAP91***	synapse	0.893265	5.185282	2.16E-07	12.1	82.9	62.9
2	rs2914983	1.10E-14	197256700…199299078	***SF3B1***	epigenetic	0.888092	7.256793	3.96E-13	33.8	123.1	130.4
3	rs75968099	5.16E-11	36034966…38107017	*MLH1*	epigenetic	0.877109	6.376857	1.81E-10	11.9	22.7	24.9
16	rs3814883	8.82E-15	28952638…30984212	***TMEM219***	signaling	0.846736	6.291546	3.14E-10	13.5	62.0	60.4
16	rs381488	8.82E-	30016830…30034	***DOC2A***	synapse	0.52129	6.08833	1.14E-	2.7	20.9	9.3

	3	15	591			6	5	09			
4	rs61405217	5.39E-11	170533784…170644824	***CLCN3***	synapse	0.718835	5.771783	7.84E-09	18.6	33.7	33.4
2	rs1451488	6.72E-17	198669426…199437305	***PLCL1***	synapse	0.035058	4.910285	9.09E-07	4.4	3.5	6.2

Table 2. EpiXcan prioritization of PGC3 SCZ-GWAS genes. Genes annotated as epigenetic/regulatory (blue) and signaling (red) for pathway studies.

GENE	Annotated Function	Rank	z-score	ATACseq annotation	H3K27ac annotation	H3K4me3 annotation	H3K27ac annotation (neuron)	gRNAs
NEK4	serine/threonine protein kinase	1	8.64	NA	Promoter	NA	Promoter	10
PLCL1	inositol phospholipid signaling	2	7.20	NA	Distal Intergenic	Promoter	Intron	10
UBE2Q2L	pseudogene	3	6.89	NA	Promoter	Promoter	Promoter	10
NAGA	lysosomal enzyme	4	6.67	NA	Promoter	Promoter	NA	10
FES	tyrosine-protein kinase	5	6.63	NA	Promoter	Promoter	NA	10
CALN1	calcium signaling	6	6.57	NA	Intron	Promoter	Intron	10
CSPG4P11	pseudogene	pseudogene	6.29	NA	Promoter	NA	3’ UTR	
ZNF804A	transcription factor	7	6.27	NA	Promoter	Intron	NA	10

FIGURES

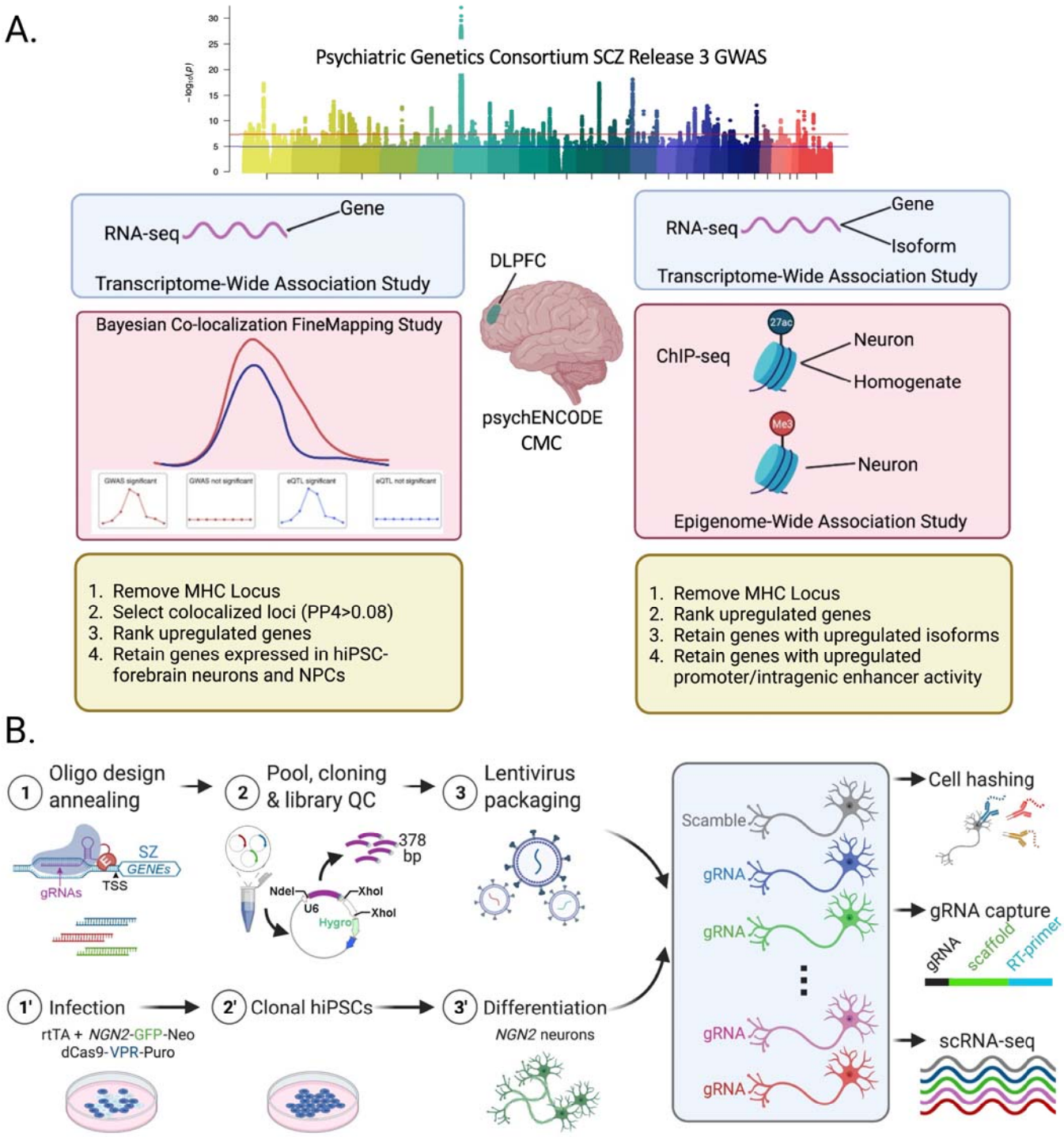

Figure 1. *ECCITE-seq (Expanded CRISPR-compatible Cellular Indexing of Transcriptomes and Epitopes by sequencing) allows perturbation of multiple eGenes in parallel to examine the transcriptional impact of each.* **(a)** Workflow for prioritization of SCZ eGenes from PGC3-GWAS by transcriptomic imputation, colocalization, and epigenome-wide associations. **(b)** Design of SCZ-GWAS gene CRISPRa gRNA library. First, designed oligos are annealed, pooled, and cloned into a plasmid backbone (1,2). Following cloning, plasmids are digested and ~ 378bp fragment contain gRNA is sequenced to determine the distribution of gRNAs in the pool (Supplementary Figure 1c-d). (3) The final library is packaged into a lenti-viral vector allowing for integration into cultured glutamatergic neurons. (1', 2') hiPSCs are first clonalized with a dox-inducible NGN2 transgene and the puromycin resistant CRISPR dCas9-VPR system. (3') Application of doxycycline induces

glutamatergic neuronal development and antibody selection results in relatively pure populations of dCas9-expressing glutamatergic neurons ready for the gRNA library. Created with BioRender.com. Partial eQTL image modified from Barbeira et. al 2018.

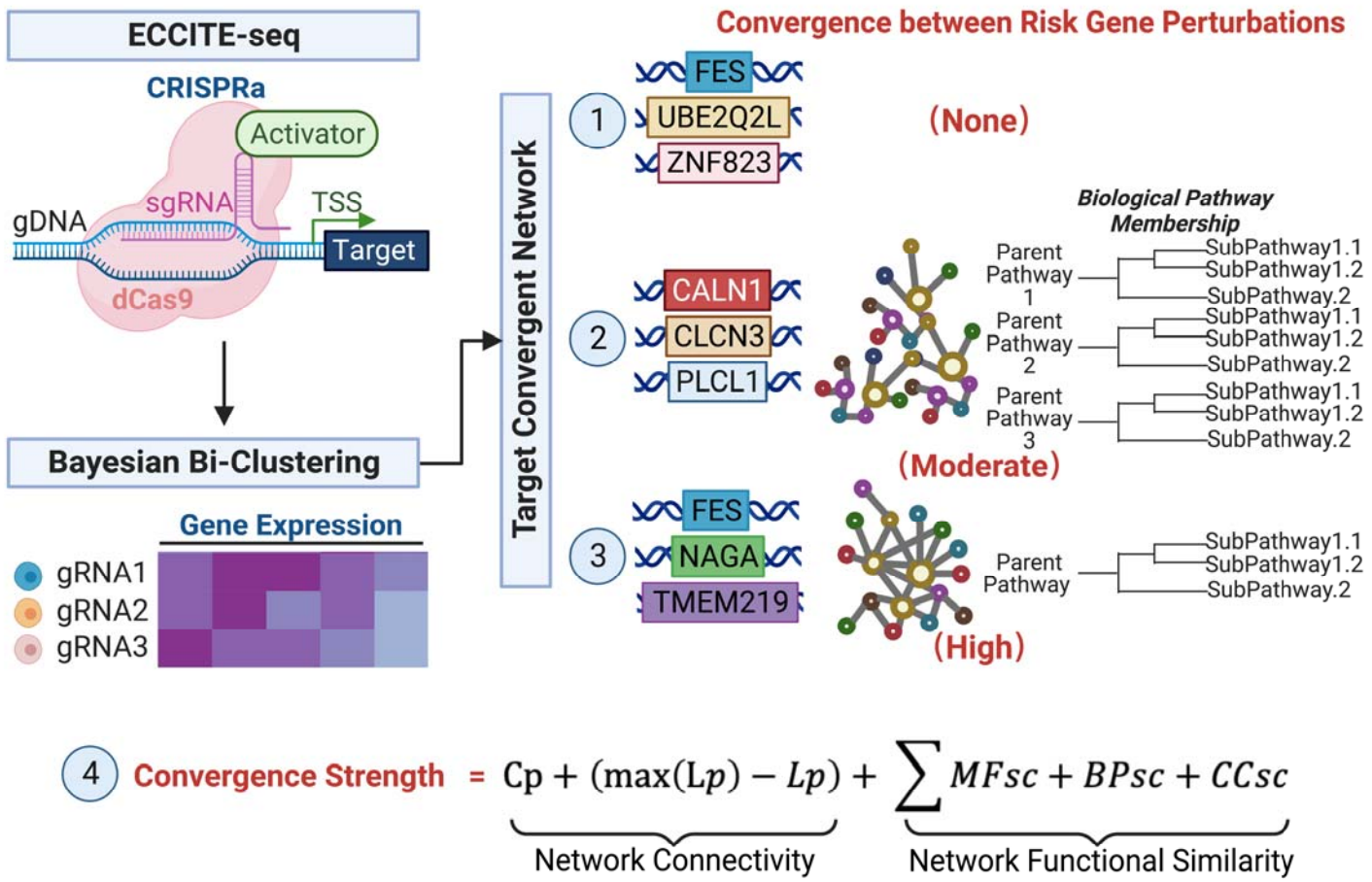

Box 1: Defining convergence and calculating convergent network strength.

Here we define convergence as the independent development of transcriptomic similarities between separate "gene perturbations" that move towards union or uniformity of biological function. Bayesian bi-clustering identifies co-expressed genes that are shared across the downstream transcriptomic impacts of any given eGene perturbations, thus, the resolved networks are the transcriptomic similarities between distinct perturbations**.** While bi-clustering resolves convergent gene co-expression networks, the strength of convergence within a network can be defined by (i) the degree of network connectivity as define by two small-world network connectivity coefficients (edge density and average path length) and (ii) the degree of functional similarity or unity between genes represented within the network. Given this definition, **(1)** represents perturbations with no convergent downstream effects, **(2)** represents a network with a moderate degree of convergence because it (i) has resolved gene co-expression clusters that can be constructed into a network, (ii) has a moderate degree of network connectivity and (ii) is enriched in biological pathways with some redundancy, while **(3)** represents a highly convergent network because the degree of network connectivity is stronger and there is greater uniformity in biological pathway gene membership. Overall, we quantify the strength or degree of convergence using the function in **(4)**, where *Cp* is the edge density (the proportion of edges present given all possible edges) and *Lp* is the average path length (the mean of the shortest distance between each pair of nodes), *MFsc* is the average semantic similarity score between each pair of nodes in the network based on Molecular Function Gene Ontology (GO), *BPsc* is the average semantic similarity score based on Biological Pathway (GO) and *CCsc* is the average semantic similarity score based on Cellular Component (GO). Semantic similarity is based on the idea that genes with similar function have similar GO annotations. Semantic similarity scores were calculated by aggregating four information content-based methods and one graph structure-based method with the R package GoSemSim. Created with BioRender.com.

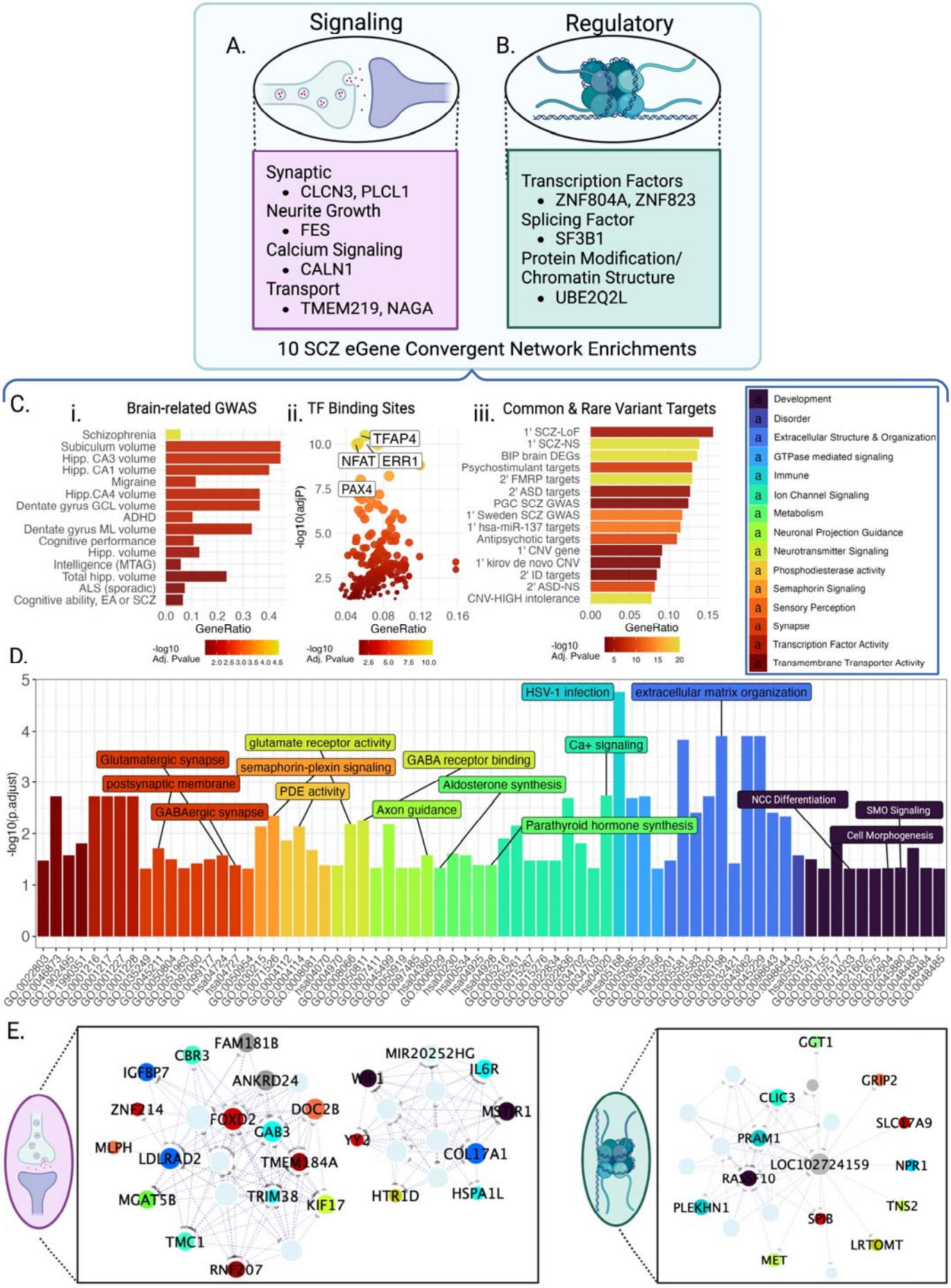
A.
Signaling
Synaptic
• CLCN3, PLCL1
Neurite Growth
• FES
Calcium Signaling
• CALN1
Transport
• TMEM219, NAGA
B.
Regulatory
Transcription Factors
• ZNF804A, ZNF823
Splicing Factor
• SF3B1
Protein Modification/
Chromatin Structure
• UBE2Q2L
10 SCZ eGene Convergent Network Enrichments
C.
i. Brain-related GWAS
Schizophrenia
Subiculum volume
Hipp. CA3 volume
Hipp. CA1 volume
Migraine
Hipp.CA4 volume
Dentate gyrus GCL volume
ADHD
Dentate gyrus ML volume
Cognitive performance
Hipp. volume
Intelligence (MTAG)
Total hipp. volume
ALS (sporadic)
Cognitive ability, EA or SCZ
GeneRatio
-log10 Adj. Pvalue
ii. TF Binding Sites
TFAP4
NFAT
ERR1
PAX4
-log10(adjP)
GeneRatio
-log10 Adj. Pvalue
iii. Common & Rare Variant Targets
1' SCZ-LoF
1' SCZ-NS
BIP brain DEGs
Psychostimulant targets
2' FMRP targets
2' ASD targets
PGC SCZ GWAS
1' Sweden SCZ GWAS
1' hsa-miR-137 targets
Antipsychotic targets
1' CNV gene
1' kirov de novo CNV
2' ID targets
2' ASD-NS
CNV-HIGH intolerance
GeneRatio
-log10 Adj. Pvalue
Development
Disorder
Extracellular Structure & Organization
GTPase mediated signaling
Immune
Ion Channel Signaling
Metabolism
Neuronal Projection Guidance
Neurotransmitter Signaling
Phosphodiesterase activity
Semaphorin Signaling
Sensory Perception
Synapse
Transcription Factor Activity
Transmembrane Transporter Activity
D.
-log10(p.adjust)
Glutamatergic synapse
postsynaptic membrane
GABAergic synapse
glutamate receptor activity
semaphorin-plexin signaling
PDE activity
Axon guidance
GABA receptor binding
Aldosterone synthesis
Parathyroid hormone synthesis
Ca+ signaling
HSV-1 infection
extracellular matrix organization
NCC Differentiation
SMO Signaling
Cell Morphogenesis
E.
FAM181B
CBR3
IGFBP7
ANKRD24
MIR20252HG
IL6R
ZNF214
FOXD2
DOC2B
GAB3
MLPH
LDLRAD2
TMEM184A
COL17A1
MGAT5B
TRIM38
KIF17
HTR1D
HSPA1L
TMC1
GGT1
GRIP2
CLIC3
PRAM1
LOC102724159
NPR1
PLEKHN1
TNS2
LRTOMT
MET

Figure 2: *Downstream target-convergent networks identified by Bayesian bi-clustering resolve distinct networks enriched for SCZ common and rare variant target genes and transcription factor binding motifs.* SCZ eGene general function as **(A)** signaling or (**B)** regulatory genes. **(C)** Convergent networks resolved across the downstream transcriptomic impacts of all ten target perturbations identified 2418 convergent genes with enrichments for **(i)** brain-related GWAS genes, **(ii)** transcription factor binding sites of know SCZ-associated TFs (TFAP4, NFAT and ERR1), and **(iii)** common and rare variant target genes. **(D)** Gene set enrichment analysis of convergent genes shared across all ten eGene perturbation were significantly enriched in multiple terms related to synaptic signaling and structure, neuronal projection and development, voltage-gated ion channel signaling, phosphodiesterase signaling, and semaphoring signaling. Full enrichment results are found in Supplemental Data 4. **(E)** Unique convergent networks were resolved across signaling (left) and regulatory (right) SCZ Genes with node genes involved in synaptic signaling and immune response. Node color corresponds with general functional term found in (D), with RNA genes colored in pale blue, while node size indicates node degree, and the line thickness represents weight of the connection (calculated as the percent duplication of the connection across bi-clustering runs). Created with BioRender.com

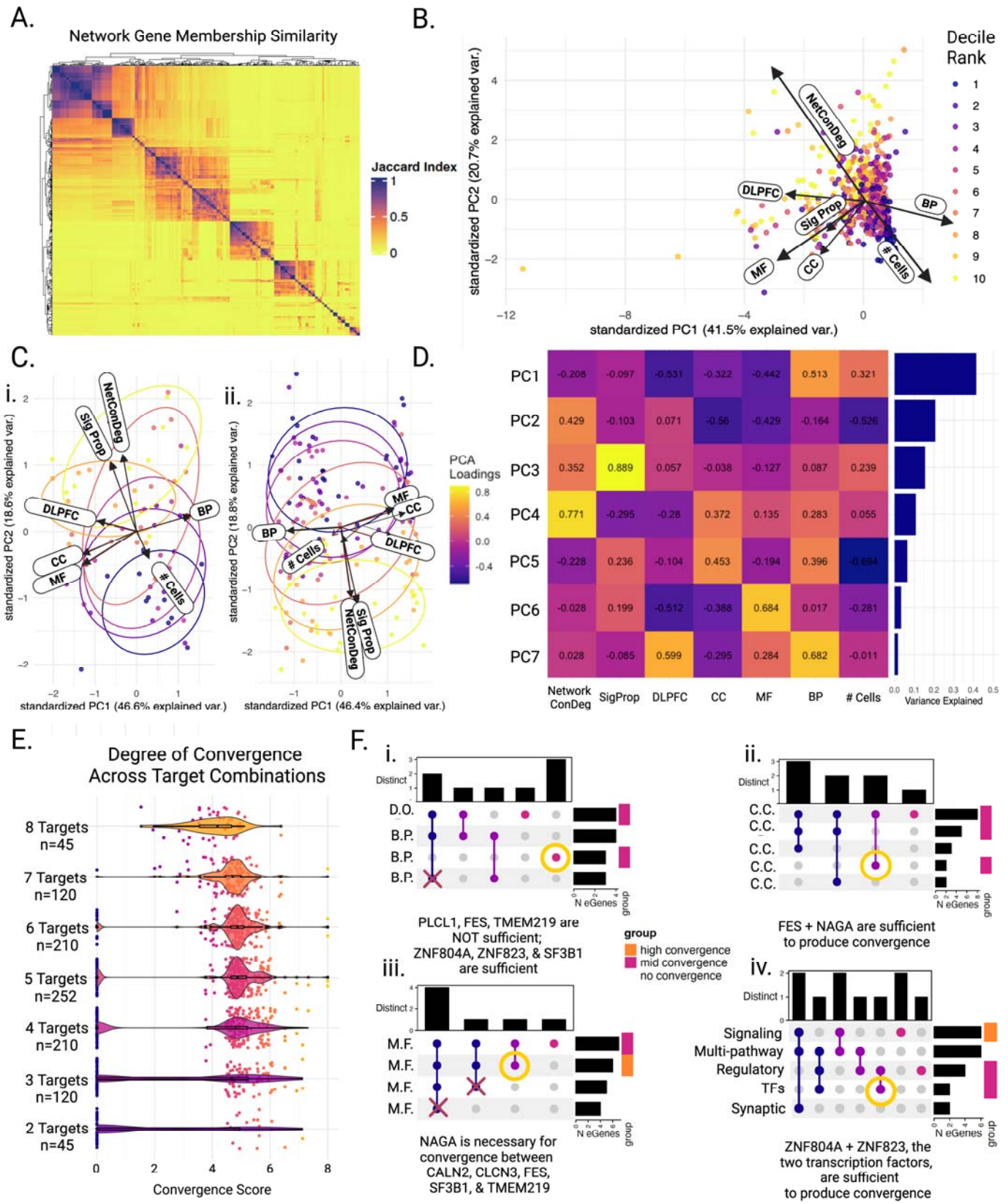

Figure 3. *The degree of network convergence is influenced by functional similarity of target perturbations.* **(A)** Heatmap of Jaccard Index Scores between every resolvable set demonstrates shared and distinct convergent effects. **(B)** Principal component analysis (PCA) of the convergence scores, the three Gene Ontology (GO) scores, DLPFC score, and Sample Size (SS) across all resolved networks reveal functional scores that have similar influence on variance as convergence. PCs 1 (x-axis) and 2 (y-axis) explain 62.2% of the variance between variables (networks). PC

loadings demonstrate the influence of each variable on variance; within the first two PCs the correlation of gene expression in the post-mortem DLPFC has a more similar level of influence of PCs 1 and 2 with variance related to convergence degree compared to other functional scores. Between PCs 2 and 3, that explains 36.2%of the variance, the relationship between DLPFC score, SS, and convergence is stronger compared to other functional scores **(Supplemental Fig. 3). (C)** Degree of convergence is influenced by network size and should be compared with networks of the same set size; PCA analysis demonstrates that the pattern of influence of signaling proportion and DLPFC score is maintained when convergence is ranked within set size (***i*** = 3 target sets; ***ii*** = 4 target sets; PC plots for the remaining sets shown in **Supplemental Fig. 4**). **(D)** Loading scores across variables (x-axis) and within PCs (y-axis) are represented in a heatmap. To the right is a paired Scree plot listing the variance explained (x-axis) by each PC (y-axis). The Signaling score, along with convergence, had the strongest influence on PC3 (15.5% variance). **(E)** Distribution of the degree of convergence (x-axis) of networks across all possible combinations of 2 to 8 target perturbations (y-axis; number of sets tested within each set ranges from 45 to 245). **(F)** Functional score and sample size explains a portion of variance related of convergence as demonstrated by PCA. **(A-C),** but not all of the variance. Identification of distinct intersections (number of intersecting genes represented by bar graph on the top x-axis) between functional sets of increasing size (y-axis, size of the set represented by matching bar graph) identify certain target pairs that are sufficient to resolve convergence alone, such as FES and NAGA **(ii;iv)**, while identifying others are not **(i)**. Additionally, some target perturbations appear necessary to resolve convergence within a set and may represent important links between SCZ risk genes **(iii)**.

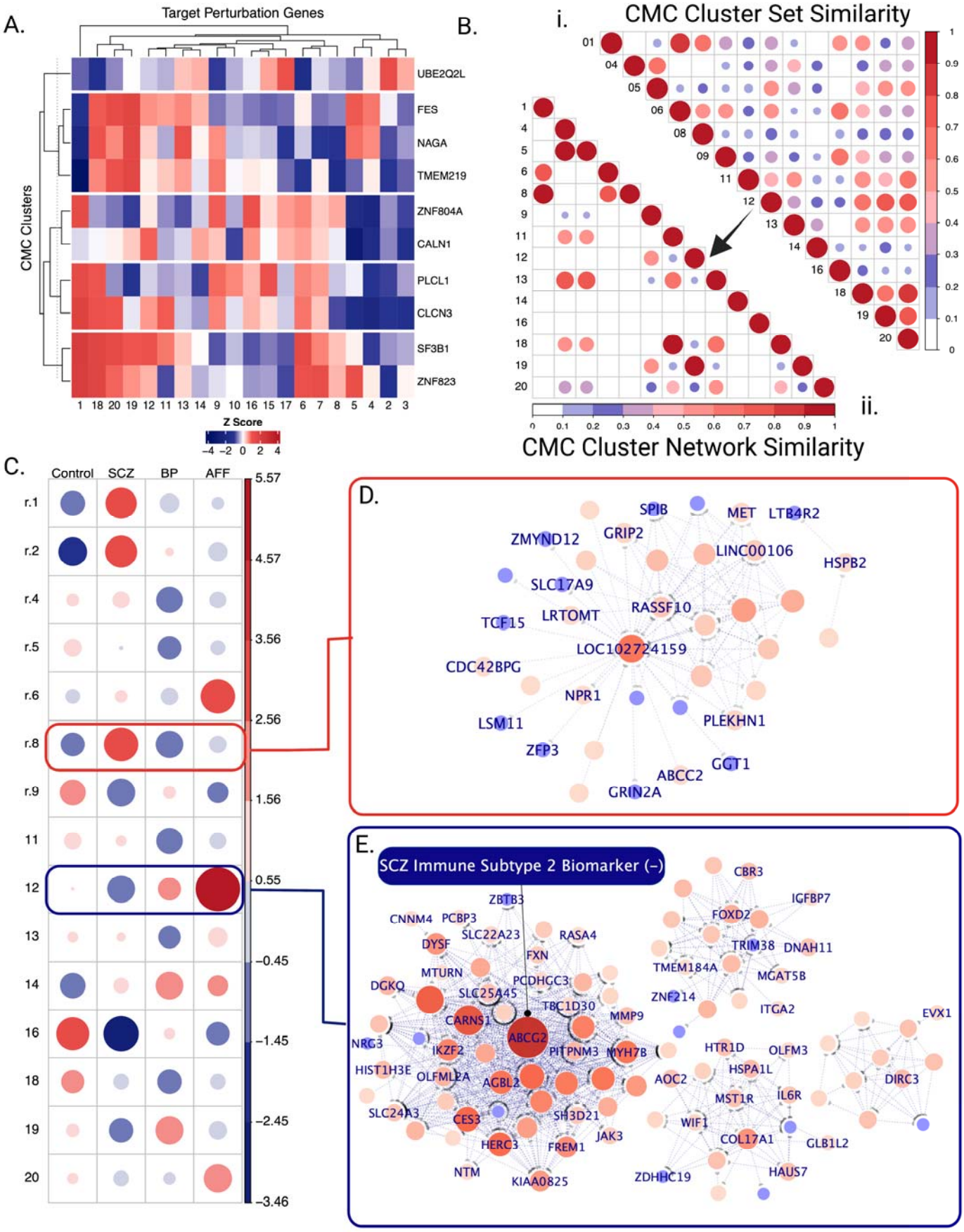

Figure 4. *Convergent networks modeling individual risk associate with diagnosis in the DLPFC.* **(A)** Heatmap of average Z-scored gene expression of the 10 ECCITE-seq target genes (columns) across

20 CMC clusters identified by K-means clustering (rows) [***** represents assigned perturbation identities in each cluster (Z-scores of >=0.025)]. **(B)** Heatmap of Jaccard Indices (0-1) demonstrating the similarity of target eGenes represented by each cluster and used to resolve convergent clusters (upper portion) matched with a heatmap of the Jaccard indices demonstrating similarity in the resulting convergent networks by cluster (lower portion). **(C)** Pearson's chi-squared test revealed significant differences in diagnosis status between clusters. The size (larger = more positive) and color (blue = negative, red=positive) of circles in the matrix represent the chi-squared residuals for diagnoses of affective disorders (AFF), bipolar disorder (BP), and schizophrenia (SCZ) (rows) for each cluster (columns). **(D)** Convergent network resolved across three regulatory eGenes (SF3B1, ZNF804A, and ZNF823), which is representative of Cluster 8 individuals. Cluster 8 is significantly associated with a SCZ diagnosis (C). **(E)** Convergent network resolved across four signaling eGenes (FES, NAGA, CALN1, CLCN3) and two regulatory eGenes (SF3B1 and ZNF804A) and that is representative of Cluster 12 individuals. Cluster 12 is significantly associated with AFF diagnoses (D). Nodes that are known targets of common or rare variants, drug targets, or known eGenes associated with neuropsychiatric disorders are labeled for both networks. Of note, the top node gene in the Cluster 12 convergent network is *ABCG2*, which is important in drug transport and blood-brain barrier permeability. Recently, relative under-expression of *ABCG2* in the blood of SCZ patients has been identified as a potential biomarker of SCZ immune type II.

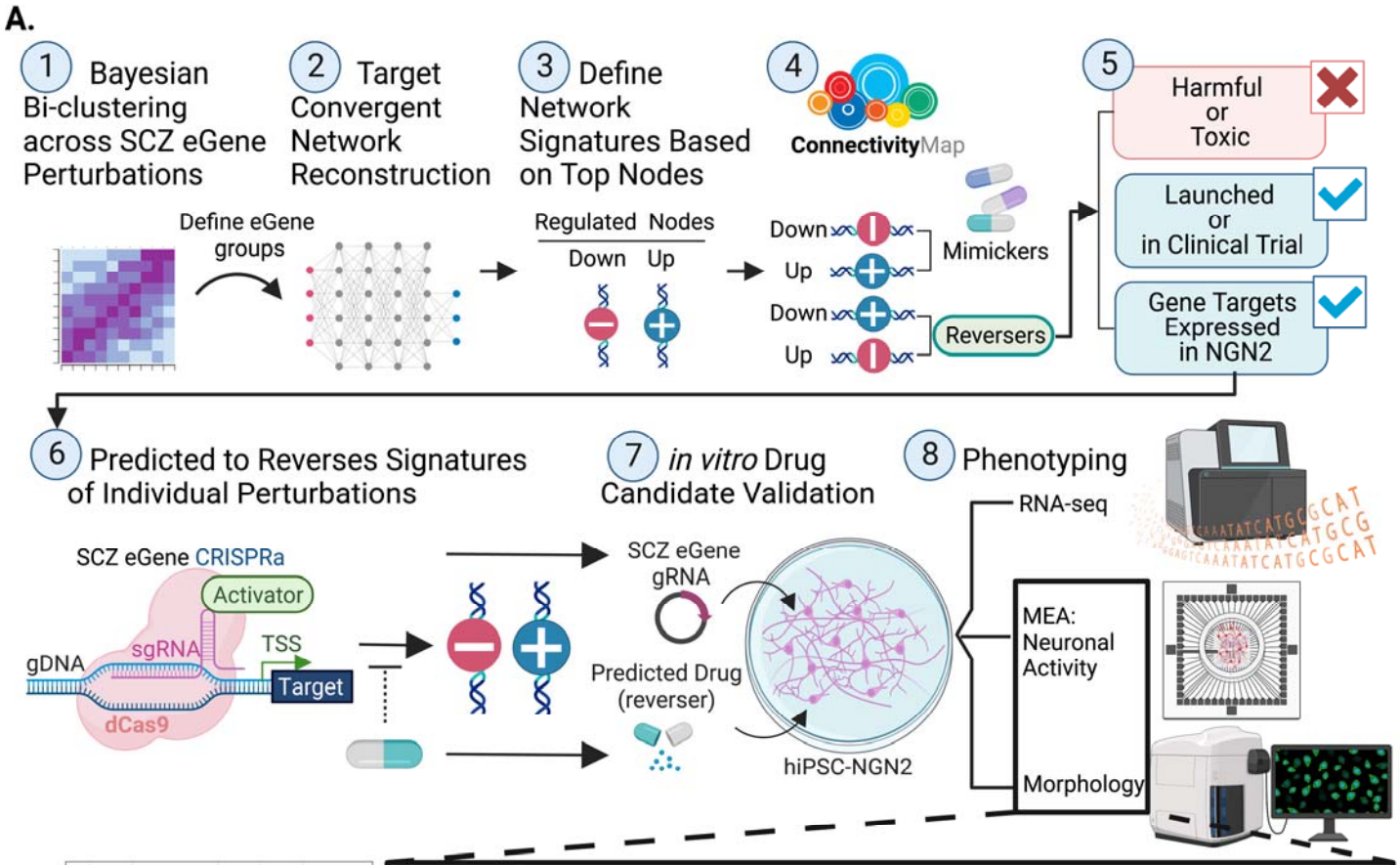

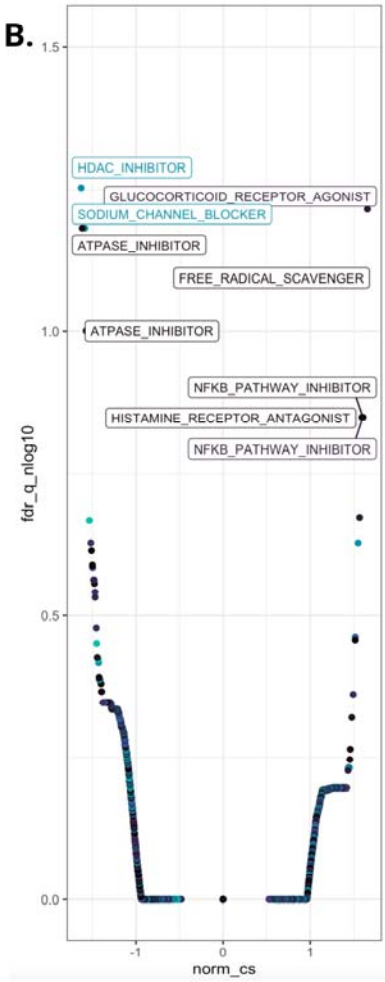

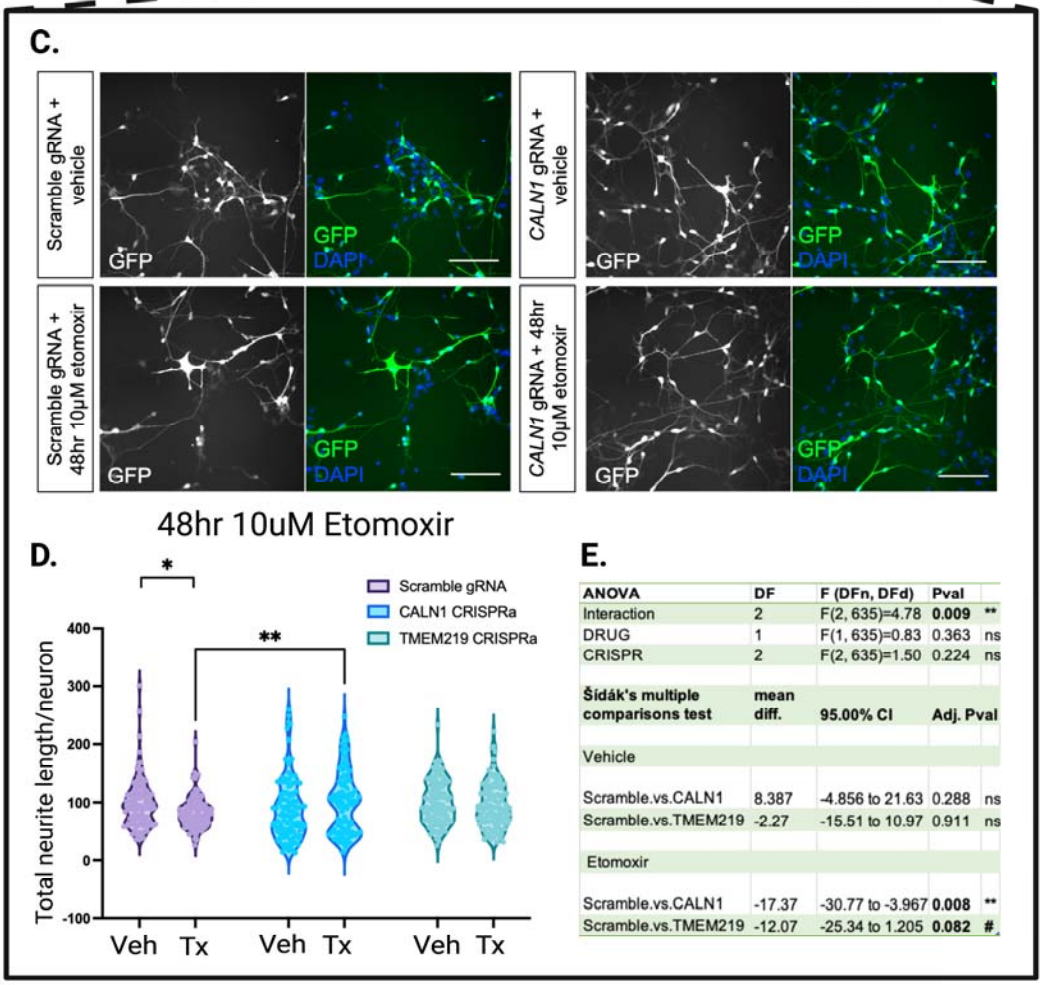

E.

ANOVA	DF	F (DFn, DFd)	Pval	
Interaction	2	F(2, 635)=4.78	**0.009**	**
DRUG	1	F(1, 635)=0.83	0.363	ns
CRISPR	2	F(2, 635)=1.50	0.224	ns
Šidák's multiple comparisons test	**mean diff.**	**95.00% CI**	**Adj. Pval**	
Vehicle				
Scramble.vs.CALN1	8.387	-4.856 to 21.63	0.288	ns
Scramble.vs.TMEM219	-2.27	-15.51 to 10.97	0.911	ns
Etomoxir				
Scramble.vs.CALN1	-17.37	-30.77 to -3.967	**0.008**	**
Scramble.vs.TMEM219	-12.07	-25.34 to 1.205	**0.082**	#

Figure 5: *In vitro validation identifies opposing effects of in silico drug predictions and top schizophrenia risk eGenes.* (**A**) Workflow of drug prioritization using LINCS drug database. (1) Bayesian bi-clustering performed across all 10 eGene perturbations identifies gene expression shared across all perturbations. (2) Un-supervised target convergent network reconstruction of the bi-clustering results resolves network relationships of convergent genes. (3) Top 150 up-regulated and down-regulated nodes identified by TCN reconstruction were used to define a network signature. (4) Network signatures were input into the Broads Institute's Connectivity Map query tool to predict drugs and perturbagens that mimic or reverse the target network signature. (5) Drugs that reversed the convergent network signature where filtered based on CS scores less than -1.00 in both neuronal (NEU) and neural progenitor cell (NPC) culture. Top drugs were filtered based on repurposing potential (Launched or in clinical trial), neurotoxicity and negative side effects, and expression of target genes in hiPSC-derived *NGN2*-neurons. (6) Following drug prioritization, their capacity to reverse individual perturbation signatures (based on the top up -and down-regulated genes) was assessed and eGene perturbations most likely to be reversed by the prioritized drugs were used in validation experiments *in vitro*. (7) CRISPR activation experiments of prioritized (based on CS score and significance in NEU and NPC culture) were carried out in hiPSC-NGN2 excitatory neurons treated with matched drug reversers for 48hrs. (8) Following CRISPRa and drug treatment, phenotypic assays (i.e. multi-electrode array (MEA) for neuronal activity; High-resolution microscopy for morphological measurements) to assess the impact of (i) perturbation, (ii) drug treatment, and (ii) perturbation by drug treatment on morphology, activity, and downstream gene expression of glutamatergic neurons were performed. **(B)** Drug-class enrichments predicted to mimic or reverse the signature of the top convergent node genes shared across all ten eGenes. **(C-E)** In vitro validation of drug-eGene phenotypic interactions. **(C)** Imaging of Day 21 *NGN2*-neurons 48hrs after treatment with 10µM etomoxir or vehicle after CRISPR activation of CALN1 (compared to scramble gRNA control). Scale bar = 100 µm. **(D)** 48-hour treatment with the small-molecule inhibitor of fatty acid oxidation (FAO) etomoxir significantly reduced neurite length in scramble control NGN2 neurons (Tukey's multiple comparisons test; Adj. Pval=0.0162). Up-regulation of SCZ eGene CALN1 significantly rescued the effect of etomoxir, demonstrating opposing effect of the drug etomoxir and CALN1 activation (Adj. Pval=0.008). Additionally, up-regulation of SCZ eGene TMEM219 demonstrated a nominal opposing effect to etomoxir (Adj. Pval=0.082) Volcano plots of total neurite length in CRISPRa Scramble/CALN1/TMEM219 gRNA cells 48hrs after treatment with 10µM etomoxir or vehicle. **(E)** ANOVA results table from a two-way Grouped ANOVA and Sidak's multiple comparisons test of the interactive effects of CRISPRa perturbation and treatment with 48hr 10µM etomoxir. Created with BioRender.com